https://doi.org/10.5194/egusphere-2026-4349
Preprint. Discussion started: 25 August 2026

Contrasting sea ice thickness variability in Arctic pack ice and marginal ice zone through ocean–sea-ice reanalyses

Francesco Cocetta[1], Doroteaciro Iovino[1], Andrea Cipollone[1], and Daniela Flocco[2, 3]

[1]CMCC Foundation - Euro-Mediterranean Center on Climate Change, Bologna, Italy
[2]Dipartimento di Scienze della Terra, dell'Ambiente e delle Risorse, Università degli Studi di Napoli "Federico II", Napoli, Italy
[3]Consorzio Nazionale Interuniversitario per le Scienze del Mare - CoNISMa, Rome, Italy

Correspondence: Francesco Cocetta (francesco.cocetta@cmcc.it)

Abstract. Rapid changes in the Arctic sea ice, including widespread thinning, loss of multiyear ice, and shifts in the seasonal cycle, provide compelling evidence of an ongoing transition toward a new Arctic climate state. While the expansion of the marginal ice zone (MIZ) has been extensively documented using concentration-based metrics, much less is known about how sea-ice thickness (SIT) variability differs between marginal and consolidated ice regimes, and how these differences relate to upper-ocean conditions. This study investigates the seasonal and interannual variability of SIT within the Arctic MIZ, and contrasts it with that of the more consolidated and less mobile pack ice, using a multi-decadal ocean–sea ice reanalysis ensemble together with satellite-derived and observation-based datasets. A regional framework is adopted to account for the strong spatial heterogeneity of Arctic sea ice and to complement the pan-Arctic analysis. Furthermore, the relationship between SIT and surface ocean conditions beneath the ice is examined. The Global Ocean Reanalysis Ensemble Product (GREP) from the Copernicus Marine Service provides a physically consistent, spatially and temporally complete framework that integrates sea-ice and ocean properties, enabling a coherent investigation of their coupled variability beyond what can be achieved using fragmented satellite observations or sparse in situ measurements alone. Analysis of the GREP ensemble reveals distinct seasonal and regional thinning patterns in the MIZ and pack ice. Since 1993, the MIZ has experienced a pan-Arctic July thinning trend of -0.14 m/decade, with regional trends ranging from -0.09 m/decade in the Barents-Kara seas sector to -0.26 m/decade in the Laptev-East Siberian seas sector. By contrast, pack ice exhibits stronger and more spatially uniform thinning throughout the year. Sea surface temperatures beneath the MIZ are systematically warmer and more variable than beneath pack ice, underscoring the importance of accounting for sea-ice heterogeneity when assessing Arctic change. These findings demonstrate that the expanding MIZ has become an increasingly important component of Arctic climate variability and that its evolution cannot be inferred from pack-ice behavior alone. Its strong regional sensitivity to oceanic forcing underscores the need to accurately represent ice-type variability and marginal-ice processes in climate models, both to constrain model biases and to improve predictions of the future Arctic sea-ice cover. Integrating ocean variables into this framework offers a robust pathway for identifying MIZ-specific indicators of the evolving Arctic climate state.

https://doi.org/10.5194/egusphere-2026-4349
Preprint. Discussion started: 25 August 2026

1 Introduction

In recent decades, Arctic sea ice has undergone profound changes beyond the well-documented decline in its extent. These include widespread thinning (Sumata et al., 2023), loss of multi-year ice (Babb et al., 2023), and shifts in the timing and structure of the seasonal cycle (Frew et al., 2025). Together, these changes provide evidence of an ongoing transition toward a new Arctic climate regime. Their implications span a wide range of Earth system scales, from local scale, where the loss of multi-year ice enhances primary production (Vancoppenolle et al., 2013), to the climate scale, where the sea-ice albedo feedback enhances shortwave radiation absorption as sea ice retreats (Goosse et al., 2018). Within this evolving system, the Arctic marginal ice zone (MIZ), defined as the transition region between consolidated pack ice and open ocean, has become an increasingly important component of the sea ice cover. Its fractional area has expanded rapidly in the last decades (Cocetta et al., 2024; Horvat, 2021) and is projected to continue increasing under future climate scenarios (Selivanova et al., 2024). Recent work has also highlighted a broader reorganization of Arctic sea-ice regimes, with several regions shifting away from the historically dominant permanent-ice state toward more seasonal and transitional regimes (Simon et al., 2025).

As the Arctic sea-ice cover transitions toward thinner, more seasonal and heterogeneous conditions, the MIZ is no longer a peripheral component of the ice cover, but an increasingly prominent driver of sea-ice variability and ocean-ice-atmosphere interactions. This evolution challenges the use of traditional diagnostic metrics originally designed for thick and compact ice. For example, the widely used sea-ice extent (SIE) metric tends to overestimate the effective ice-covered areas in the MIZ, where low-concentration and fragmented ice conditions dominate, because it treats marginal and pack ice equally (Matthews et al., 2020; Notz, 2014). Similarly, state-of-the-art sea-ice thickness (SIT) retrievals remain affected by substantial uncertainties in thin-ice conditions, a common and characteristic feature of the MIZ expected to become increasingly prevalent. Furthermore, satellite coverage remains limited during the melt season, when the MIZ reaches its maximum spatial extent (Cocetta et al., 2024; Frew et al., 2025). Although recent advances in hybrid reconstruction methods are improving the temporal consistency of Arctic SIT datasets and helping reduce observational gaps (Edel et al., 2025), the characterization of thickness variability in the MIZ remains far less mature than that of concentration-based sea-ice properties.

Previous investigations of Arctic MIZ variability have primarily focused on sea-ice concentration, extent, or areal metrics. Therefore, the ongoing transition toward a more seasonal and fragmented Arctic sea ice has largely been characterized through changes in ice coverage rather than changes in ice thickness. Yet sea-ice thinning is a defining feature of the ongoing Arctic sea-ice change (Sumata et al., 2023) and directly influences ice thermodynamics, mechanical stability, atmosphere-ocean exchanges, and seasonal predictability. Understanding whether SIT evolves differently in the MIZ compared to consolidated pack ice is therefore critical for characterizing the mechanisms driving the Arctic transition. A process-based perspective on the MIZ is therefore required. In this study, the MIZ is identified as the region with sea-ice concentration (SIC) between 15% and 80%, while pack ice corresponds to SIC above the upper threshold. This threshold-based definition is widely used in large-scale studies, allowing consistent comparison of sea-ice conditions across observational products and reanalyses (Frew et al., 2025; Rolph et al., 2020; Horvat, 2021; Cocetta et al., 2024), allowing consistent comparison among sea-ice information derived from different sources. Alternative approaches based on wave-ice interactions (Horvat et al., 2020), SIC anomaly (Vichi, 2022), and

https://doi.org/10.5194/egusphere-2026-4349
Preprint. Discussion started: 25 August 2026

young-ice permeability (Mangatane et al., 2025) provide valuable complementary views of the MIZ. Nevertheless, the thickness structure of the MIZ and its coupling with the upper ocean remain insufficiently characterized, while emerging evidence indicates that incorporating SIT information substantially improves predictions of Arctic sea ice and its atmospheric impacts (Liu et al., 2025). This motivates a more explicit assessment of SIT variability across distinct sea-ice regimes, especially within the MIZ, where interactions between thin, mobile ice and the seasonally evolving surface ocean are expected to be strongest.

To address this gap, this study investigates the seasonal and interannual variability of SIT within the Arctic MIZ and contrasts it with that of the consolidated pack ice. Specifically, we examine how SIT variability differs between the two regimes, how it relates to upper-ocean temperature across seasons and Arctic sectors, and how regional processes contribute to the pan-Arctic evolution of the sea-ice cover. To this end, this analysis combines observation-derived datasets with the Global Ocean Reanalysis Ensemble Product (GREP, version 2), from the Copernicus Marine Service (CMEMS), which provides a spatially and temporally consistent assessment of both sea-ice and upper-ocean conditions at regional and hemispheric scales. We first assess the ability of available satellite SIT products to distinguish between marginal and pack ice during the growth season, when satellite observations are available. The analysis is then extended using the observation-derived dataset of Landy et al. (2022), which applies deep learning techniques to generate a pan-Arctic SIT dataset during the melt season. This multi-dataset comparison aims to evaluate the suitability of these SIT products for investigating sea-ice variability within the MIZ, investigating the differences in mean SIT between pack and the MIZ, and the discrepancies among datasets. In this context, global ocean–sea ice reanalyses provide a complementary framework by combining observations with numerical models to produce dynamically consistent estimates of sea-ice and ocean conditions over multi-decadal timescales. Previous studies have demonstrated that GREP reliably represents concentration-based sea-ice properties (Iovino et al., 2022; Cocetta et al., 2024). Here, we extend this evaluation to the representation of SIT, characterizing MIZ thickness variability in the context of changing sea-ice area and the underlying ocean temperature. Overall, the analysis performed at the pan-Arctic scale highlights that investigating Arctic sea ice beyond extent-based metrics requires explicit consideration of ice heterogeneity through process-based classifications. The integration of sea-ice and surface-ocean variables in GREP enables us to assess how SIT differs between pack ice and the MIZ, and how these regimes relate to sea surface temperature, SST, beneath the ice. This is especially relevant in the Arctic, where direct observations of ocean temperature under sea ice are sparse and often indirect (Donlon et al., 2007; Emery et al., 2001), and where regional ocean heat content has been shown to play a major role in modulating sea-ice variability (Bianco et al., 2024; Perovich et al., 2008).

A regional perspective is central to this analysis because Arctic sea-ice and upper-ocean conditions exhibit strong spatial heterogeneity. The Arctic Ocean is therefore divided into four sectors characterized by distinct seasonal sea-ice and MIZ behavior. These sectors approximately separate regions dominated by perennial Arctic sea ice, Pacific inflow influence, eastern Siberian shelf processes, and Atlantic inflow influence. This framework allows us to explicitly assess the role of regional heterogeneity in controlling SIT variability and ocean-sea ice coupling, and provides a clearer picture of the contribution of each Arctic sector to the hemispheric-scale signal. By combining thickness, ice-type classification, and upper-ocean thermal conditions, this framework provides a new perspective on Arctic sea-ice change that extends beyond traditional extent-based diagnostics, and helps identify emerging indicators of the evolving Arctic climate state.

https://doi.org/10.5194/egusphere-2026-4349
Preprint. Discussion started: 25 August 2026

This study is then structured as follows: Section 2 describes the datasets and methods, detailing GREP, the observation-based datasets, and the definition of the Area Fraction (AF) metric used to quantify marginal and pack ice covers. Section 3 presents the pan-Arctic analysis of SIT and SST beneath sea ice, including their seasonal cycles, probability distributions, and mutual relationships. Section 4 examines the regional variability of these properties and their decadal trends. The results are discussed in Section 5, and the main conclusions are summarized in Section 6.

2 Data and methods

This study combines global ocean-sea ice reanalyses, satellite-based products, and observation-derived datasets to investigate the variability of Arctic SIT within the marginal ice zone and its relationship with surface ocean conditions. The analysis focuses on monthly mean sea-ice thickness, sea-ice concentration, and ocean temperature beneath sea ice, and compares conditions in the MIZ and consolidated pack ice. The MIZ is identified using a sea-ice concentration threshold-based definition that enables a consistent classification across observational products and reanalyses, and its variability is assessed at both pan-Arctic and regional scales from 1993 to 2020.

2.1 Global ocean reanalysis

The analysis is primarily based on GREP (version 2), which comprises four ensemble members. GREP has been previously used to analyze sea-ice states and their variability in both hemispheres (Iovino et al., 2022; Cocetta et al., 2024), and it covers the period 1993-2020. Although the more recent GREP version (European Union-Copernicus Marine Service, 2019) extends the temporal coverage to 2024, the larger ensemble size of GREPv2 was considered more suitable for climate-oriented analyses. In this study, we consider monthly ensemble means of sea ice concentration (SIC) and SIT north of 66°N, together with ocean temperature beneath sea ice. For selected analyses, variables from individual members are also considered.

The four GREP ensemble members are C-GLORS version 7 (Storto et al., 2016), FOAM-GloSea5 version 13 (MacLachlan et al., 2014), GLORYS2 version 4 (Lellouche et al., 2013), and ORAS5 (Zuo et al., 2019). All reanalyses are based on the NEMO ocean model (Nucleus for European Modelling of the Ocean; https://www.nemo-ocean.eu/), although using different model versions and parameterizations, and all share the global tripolar ORCA025 grid at eddy-permitting resolution. The horizontal resolution is approximately 1/4° with 75 vertical levels. In all members except FOAM-GloSea5v13, sea ice is simulated with the LIM2 sea-ice model (Fichefet and Maqueda, 1997; Goosse and Fichefet, 1999), which employs a single sea ice thickness category. FOAM-GloSea5v13 instead uses the CICE4.1 sea-ice model (Hunke and Lipscomb, 2010), which includes a sea ice thickness distribution. Sea-ice dynamics are described using elastic–viscous–plastic rheology (EVP; Hunke and Dukowicz (1997)) in all reanalyses except for ORAS5, whose LIM2 implementation adopts a viscous–plastic (VP) formulation.

Differences among the GREP members also arise from their data assimilation (DA) schemes, including observation operators, background error covariances, assimilation windows, as well as the ingested observational datasets. A comprehensive summary of the differences among ensemble members in assimilating ocean and sea-ice variables is provided in Table 1 of Cocetta

https://doi.org/10.5194/egusphere-2026-4349
Preprint. Discussion started: 25 August 2026

et al. (2024). In the sea-ice sector, all members adopt univariate approaches, assimilating SIC through different data sources. GLORYS2v4 ingests IFREMER CERSAT SSM/I SIC (Ezraty et al., 2007) at 12.5 km resolution, while ORAS5 assimilates CMS OSTIA SIC (product SST_GLO_SST_L4_REP_OBSERVATIONS_010_011, 0.05° resolution), using reprocessed data prior to 2008 and near-real-time analyses thereafter. The remaining ensemble members, C-GLORSv7 and FOAM-GloSea5v13, assimilate OSI SAF SIC (product OSI-450-a, OSI SAF (2022); Lavergne et al. (2019)), albeit with different assimilation windows. Recent advances towards multivariate assimilation have been documented by adding sea-ice thickness measurements (see, for example, Cipollone et al. (2023) for C-GLORS, Mignac et al. (2022) for FOAM). However, these developments are not included in the current GREP version (Desportes et al., 2022). This limitation provides an opportunity to assess the ability of individual GREP members, as well as their ensemble mean, to represent SIT as an outcome of the modeled sea-ice processes, without direct observational constraints.

2.2 Satellite-based sea ice thickness observations and derived products

Arctic SIT from GREP is compared against a set of satellite-derived datasets available from October 2010. Since no single product provides complete and equally reliable coverage across the full annual cycle and all sea-ice regimes, three datasets are considered to assess their suitability for ice classification and to place the GREP estimates in an observational context. We consider (1) the SIT dataset derived from the European Space Agency (ESA) CryoSat-2 radar altimetry (version 2.6 at 25 km resolution; Hendricks and Paul (2023)). This product is effective in determining SIT thicker than 0.5 m (Zygmuntowska et al., 2014) by relying on snow depth climatology (Warren et al., 1999) and the hydrostatic equilibrium assumption (Ricker et al., 2014; Tilling et al., 2016). Then (2), we use SIT computed from the ESA SMOS (Soil Moisture and Ocean Salinity; Tian-Kunze et al. (2014)) satellite. Being derived from a passive microwave radiometer (Huntemann et al., 2014), SMOS prioritizes thin SIT, roughly up to 0.5 m, by evaluating brightness temperature in the L-band frequency (Kaleschke et al., 2010). We use version 3.6 at 12.5 km resolution, which features an updated Radio Frequency Interference (RFI) filtering scheme that extends data coverage in the Arctic.

In addition (3), we consider the CS3SMOS dataset (version 300; Ricker et al. (2017)), which combines CryoSat-2, SMOS, and Sentinel-3 observations. This product builds upon the merged CryoSat-2 and SMOS dataset (CS2SMOS) used in Cocetta et al. (2024)[1], but incorporating SIT estimates from Sentinel-3A (available since October 2016) and Sentinel-3B (since October 2018) into the Optimal Interpolation (OI) process. The SIT measurements retrieved from Sentinel-3A/B are derived using the AWI v2.6 sea-ice freeboard and thickness retrieval algorithm, ensuring consistency with the CryoSat-2 processing. Compared with CS2SMOS, CS3SMOS is supplied at a higher spatial resolution (12.5 km instead of 25 km) and uses SMOS version 3.6. The OI algorithm combines radar altimetry and L-band radiometry while accounting for the respective uncertainties of different ice thickness classes (Kaleschke et al., 2015). Here, sea ice concentration from CS3SMOS is also used.

To extend the analysis into the melt season, when satellite-based SIT products are more limited, and the MIZ reaches its maximum spatial development, the biweekly Arctic SIT dataset described by Landy et al. (2022) is also used. This observation-derived product, provided by the British Antarctic Survey (BAS), spans May 2011 to July 2020, at 80 km spatial resolution, and

[1]Reference is the same as CS3SMOS, Ricker et al. (2017)

https://doi.org/10.5194/egusphere-2026-4349
Preprint. Discussion started: 25 August 2026

it is based on deep learning and CryoSat-2 radar response simulations. Associated uncertainty estimates are included. During the melt season, a one-dimensional convolutional neural network trained on optical and synthetic aperture radar (SAR) imagery is applied to improve lead detection from radar waveforms using optical and synthetic aperture radar imagery, enabling a year-round estimate of Arctic SIT (Dawson et al., 2022). Radar waveforms are processed using the SAMOSA+ analytical model, and freeboard estimates are corrected for electromagnetic range bias. Sea ice thickness is then derived from freeboard using auxiliary information on ice concentration, ice type, and snow properties. This dataset is particularly valuable for evaluating the seasonal continuity of thickness evolution beyond the freezing season, despite its coarser spatial resolution.

2.3 Observation-based ocean surface temperature

Ocean temperatures at the sea ice-ocean interface, used for comparison with GREP, is obtained from the NOAA 0.25° Daily Optimum Interpolation Sea Surface Temperature dataset (OISST v2.1; Huang et al. (2021)). Since direct satellite retrievals of sea surface temperature (SST) are not available in ice-covered regions and in situ observations remain sparse, the SST beneath the ice is empirically derived from surrounding observations via a regression-based approach. SIC used to identify ice-covered grid cells is provided by NASA's Goddard Space Flight Center up to 2004, and by NCEP (National Centers for Environmental Prediction) thereafter. In partially ice-covered grid cells, a smooth transition between open-water SST estimates and freezing-point temperature values is achieved by incorporating the prescribed freezing-point constraint within the optimal interpolation framework, together with satellite and in situ observations. This approach provides a spatially consistent SST field and avoids unrealistically warm temperatures beneath sea ice (Banzon et al., 2022).

2.4 Area Fraction

The spatial extent of pack and MIZ is quantified using the area fraction (AF), defined as the percentage of the total Arctic sea-ice area (SIA) occupied by a given ice type. For the MIZ, this metric is equivalent to the marginal ice zone fraction (MIZF) introduced in Horvat (2021). Notably, the SIA is used instead of sea-ice extent (SIE) to reduce the overestimation of sea-ice cover when assessing the MIZ.

Figure 1 compares the seasonal cycles of SIA and SIE from GREP for total ice, pack ice, and the MIZ, while showing their relative differences expressed as percentages. The seasonal cycles exhibit similar shapes, with consistent timing of extremes and comparable slopes. However, the relative difference is non-negligible for the total ice during summer, reaching approximately 40% in July. This signal is dominated by the MIZ presence, which represents a substantial source of uncertainty throughout the year (Fig. 1b). The relative difference always exceeds 75% and peaks at more than 120% in October, coinciding with the secondary maximum in marginal ice cover. As expected, the difference between SIA and SIE is significantly smaller for pack ice.

https://doi.org/10.5194/egusphere-2026-4349
Preprint. Discussion started: 25 August 2026

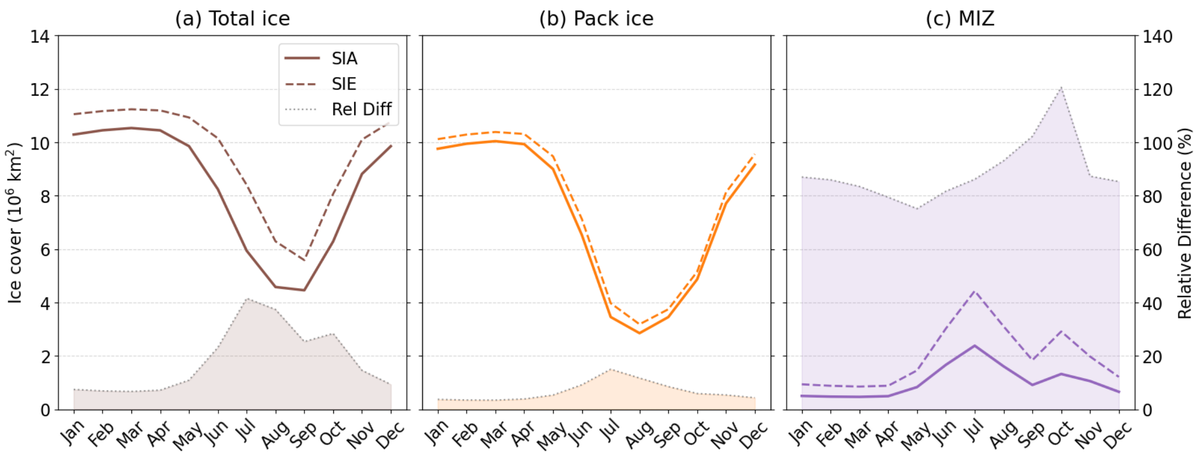

Figure 1. Seasonal cycles of SIA and SIE for Total ice cover (a), Pack ice (b), and the MIZ (c) from GREP. Relative difference (shade) between the two metrics is also shown.

3 Hemispheric-scale results

The seasonal cycle of Arctic sea ice is characterized by a pronounced redistribution between pack-ice and MIZ conditions. During summer, melting and fragmentation promote the expansion of the MIZ, whereas autumn and winter are dominated by the consolidation of the ice cover. Over recent decades, this seasonal cycle has shifted toward a progressively larger summer MIZF (Cocetta et al., 2024).

Figure 2 shows the evolution of the Arctic sea-ice cover over the period 1993-2020 by separating the contributions of pack ice and the MIZ. The annual mean sea-ice area (SIA; Fig. 2a) shows a progressive decline in pack ice accompanied by a corresponding increase in the MIZ. Whereas pack ice occupied approximately twice the area of the MIZ in the early 1990s, the two categories reached comparable extents by the end of the study period. The regions where sea ice has transitioned from pack ice to MIZ are colored in green in the maps of Fig. 2b, which display the ice-type transitions between the 1993–2002 and 2011–2020 periods for the months from June through November. The widening of the MIZ occurred at the expense of the retreating pack ice, while its contraction was due to the transition from marginal to sparse ice or open ocean (indicated by the red regions). Together, these factors drive the northward migration of the MIZ observed in recent studies (Rolph et al., 2020; Cocetta et al., 2024). The monthly maps reveal that the yearly-averaged evolutions are primarily driven by changes occurring between July and October, corresponding to the season of sea ice minimum extent. The progressive replacement of pack ice by marginal ice therefore provides the large-scale framework within which changes in sea-ice thickness should be interpreted. As the Arctic transitions toward a more seasonal ice regime, understanding SIT variability across ice types becomes increasingly important for characterizing the changing state of Arctic sea ice.

To help visualize the spatial and seasonal variability of the MIZ, Fig. S1 in the Supplementary Materials provides monthly climatological maps (1993–2020) of pack ice and the MIZ in GREP, alongside the number of ensemble members identifying

https://doi.org/10.5194/egusphere-2026-4349
Preprint. Discussion started: 25 August 2026

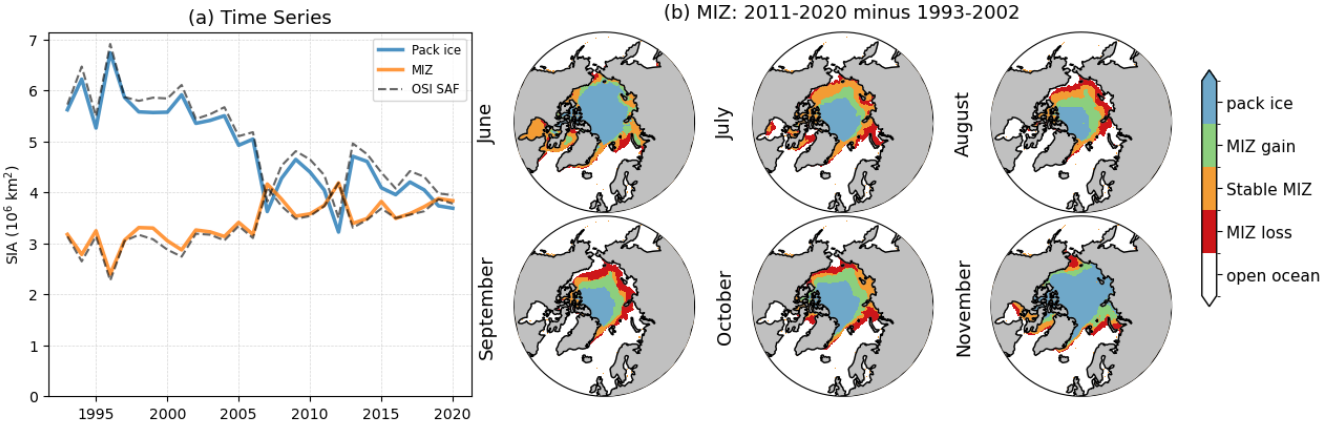

Figure 2. (a) Yearly-averaged SIA for pack ice (blue) and the MIZ (orange) from GREP, compared against the OSI SAF dataset (dashed black line) for the period 1993–2020. (b) Maps of decadal transitions of the MIZ and pack ice from June through November, comparing the 1993–2002 and 2011–2020 decades. Regions of persistent pack ice are displayed in blue, areas that transitioned to MIZ in 2011–2020 are shown in green, regions of stable MIZ are in orange, and areas that turned into open ocean or sparse ice conditions are colored in red.

MIZ conditions at each grid cell. The latter comparison shows that the GREP ensemble mean yields a more robust and spatially coherent identification of marginal ice by reducing the impact of spurious individual detections and retaining regions of high model agreement.

3.1 Sea ice thickness

Similarly to the analysis of area fraction, the GREP ensemble reveals a clear contrast between the seasonal evolution of SIT in the two ice types. The GREP time series of area-weighted mean SIT for total, pack, and the MIZ are displayed in Fig. 3a, with shadings representing the envelopes of the GREP members. While the evolution of SIT for total and pack ice exhibits similar seasonal cycles with a minimum thickness in November, the MIZ shows a distinct evolution, characterized by a minimum SIT in October and a broader maximum in early summer, typically in June or July. This difference highlights the distinct nature of the two ice regimes and indicates that MIZ thickness variability cannot be inferred from pack-ice behavior alone. Rather, pack ice and the MIZ respond differently to seasonal forcing, suggesting distinct controls on ice growth, melt, and redistribution. From 1993 to 2020, the thickness of pack ice exhibits a pronounced negative trend, comparable to that of total ice, with a mean rate of -0.29 ± 0.02 m/decade, reflecting widespread decrease across all seasons. In contrast, the SIT reduction in the MIZ is more strongly concentrated in the seasonal maximum, reaching -0.14 ± 0.03 m/decade in July, while remaining much weaker (-3.56 ± 0.96 cm/decade) in October. The spread among GREP members also differs between the two ice types. For total and pack ice, it is larger during periods of minimum thickness and smaller near the seasonal maximum, whereas in the MIZ it is the opposite.

https://doi.org/10.5194/egusphere-2026-4349
Preprint. Discussion started: 25 August 2026

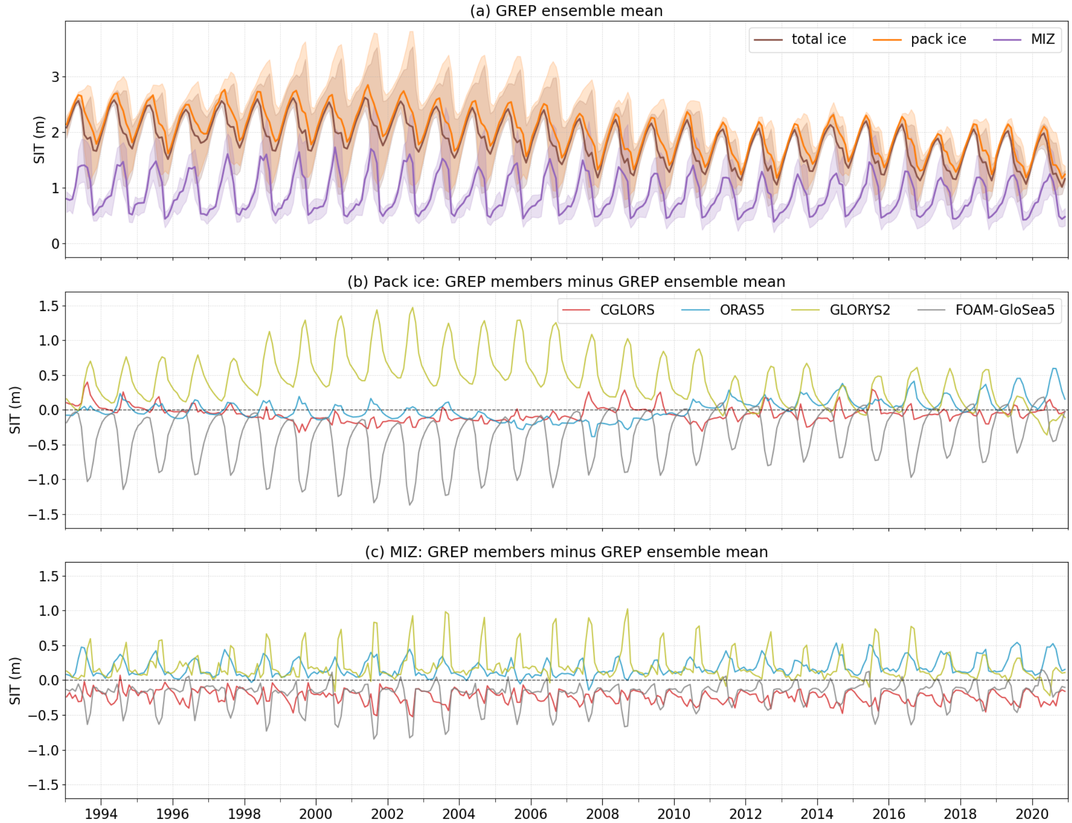

Figure 3. Time series of monthly mean SIT for total, pack, and marginal ice from the GREP ensemble mean over the period 1993–2020 (a). Shaded regions illustrate the envelope of the ensemble members. Differences in mean sea-ice thickness for pack (b) and marginal (c) ice between the GREP ensemble mean and individual members.

The spread among GREP members for total ice is primarily controlled by systematic differences in the representation of pack-ice thickness (Fig. 3b). GLORYS2 overestimates SIT compared to the ensemble mean, especially before 2010, and shows a delay of approximately one month, producing the temporal shift evident in the ensemble members' envelope in Fig. 3a. After 2011, the discrepancies between GLORYS2 and the GREP ensemble mean decrease, becoming comparable in magnitude to those of the other reanalyses. FOAM-GloSea5 shows the opposite tendency over much of the record, substantially underestimating SIT when the pack ice is thin while remaining closer to the ensemble mean near the seasonal maximum. C-GLORS and ORAS5 generally lie within the envelope bounded by these two members and do not show systematic biases throughout the full period. In the MIZ, the largest departures from the ensemble mean occur when the SIT is maximum (Fig. 3c). Over most of the analyzed period, C-GLORS and GLORYS2 simulate thinner marginal ice than the ensemble mean, whereas ORAS5 and FOAM-GloSea5 tend to simulate thicker marginal ice. Overall, these differences indicate that the GREP ensemble mean provides a more robust estimate of SIT variability than any individual member, both for the total and for the

https://doi.org/10.5194/egusphere-2026-4349
Preprint. Discussion started: 25 August 2026

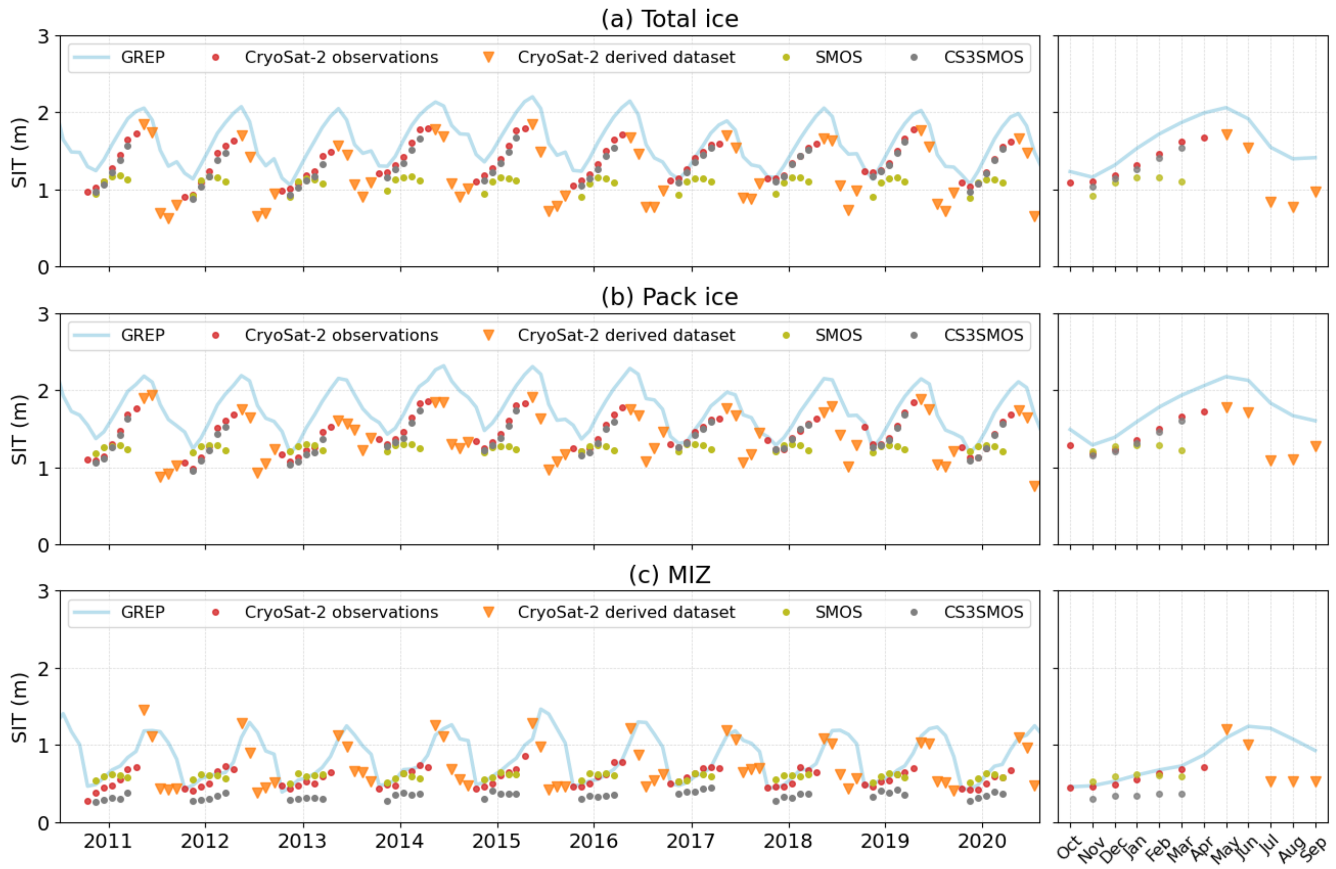

Figure 4. Time series and seasonal cycle of monthly mean SIT for total (a), pack (b), and marginal (c) ice. Estimates are shown for the GREP ensemble mean and the observational datasets (CryoSat-2, SMOS, and CS3SMOS) for winter, along with the CryoSat-2 derived dataset for the melt season. Monthly means for SMOS and CS3SMOS in October and April are excluded because the data do not cover the full months.

two sea-ice types separately. In particular, the four-member ensemble mean mitigates biases that individual reanalyses may encounter during specific periods.

We evaluate the GREP SIT against CS3SMOS, CryoSat-2, and SMOS, as well as the CryoSat-2-derived melt-season dataset. In Fig. 4, SIT time series and seasonal cycles for total ice, pack ice, and the MIZ are presented for the 2010–2020 period. During the growth season, CS3SMOS and CryoSat-2 are consistent with GREP for total and pack ice, although both show slightly weaker seasonal thickening. In contrast, SMOS is constrained by its sensitivity to thin ice and therefore cannot capture the entire thickness of the pack ice. Within the MIZ, GREP remains close to CryoSat-2 and SMOS, while CS3SMOS shows a marked low thickness relative to the other datasets, despite maintaining a monotonic thickening evolution consistent with CryoSat-2 and GREP.

https://doi.org/10.5194/egusphere-2026-4349
Preprint. Discussion started: 25 August 2026

During the melt season, the CryoSat-2–derived dataset by Landy et al. (2022) shows a seasonal evolution that differs substantially from GREP, especially in the MIZ. For total and pack ice, the derived dataset exhibits a sharper decrease in summer thickness and a late-summer recovery before reconnecting with winter CryoSat-2 estimates. GREP instead shows a more gradual thinning that extends into autumn. In the MIZ, the discrepancy is stronger: the CryoSat-2–derived dataset exhibits an abrupt increase in thickness in May and June and then nearly constant summer values comparable to those observed in winter. GREP, instead, exhibits a broad early-summer maximum followed by a progressive decline. Despite these differences in seasonal structure, the interannual variability of SIT for total and pack ice remains broadly coherent across datasets, with common low-thickness years such as 2011 at the end of summer and weak annual maxima in 2013 and 2017. The MIZ shows stronger interannual variability than pack ice across all products, especially between March and July, when the SIT peaks in the CryoSat-2 derived dataset exhibit varying seasonal profiles (e.g., sharper in 2012 and broader in 2013). The analysis indicates methodological differences and limitations in the retrieval and post-processing algorithms of SIT datasets, which contribute to persistent uncertainties in SIT estimates across seasons, regions, and ice regimes.

The seasonal distributions of GREP SIT further emphasize the differences between pack ice and the MIZ. Monthly probability density functions (PDFs; Fig. 5) for the pack ice remain relatively compact during the growth season while shifting progressively toward larger values; the peak moves from 0.78 m in November to 2.41 m in May, reflecting regular seasonal thickening. As summer approaches, the distributions broaden and the peaks weaken, indicating a more heterogeneous ice cover; during this transition, the peak shifts from 2.09 m in June toward lower thickness values. The bell-shaped distribution characteristic of the growth season reappears in October with the onset of the freezing season. In the MIZ, the distributions are confined to thinner ice during winter and early spring, reflecting the limited spatial extent of marginal ice during these months. In late spring and early summer (May and June), the MIZ develops a more pronounced thickness distribution, with a noticeable peak around 1 m in June that coincides with the annual maximum extent of the MIZ (Cocetta et al., 2024). During summer, while the MIZ remains wide, its PDFs broaden and begin to resemble those of the pack ice, although shifted toward lower values. In autumn, the occurrence of narrow, local peaks indicates that the newly formed, thin ice is again distinct from the thicker, consolidated ice that has already transitioned into the pack-ice regime. By December, the peak in the PDF weakens and the distribution begins to flatten, resembling winter conditions.

To relate the ice thickness in the MIZ and pack ice to their spatial extents, Fig. 6 shows a scatter plot of mean SIT versus AF (cf. Section 2.4), with markers representing monthly means. For most of the year, the two regimes occupy distinct regions of the scatter space. The marginal-ice cluster (solid markers) follows a well-defined C-shaped seasonal cycle. During autumn, the MIZ contracts from AF ≈ 0.2 in October to less than 0.05 in March, while mean SIT increases gradually from about 0.5 m to 0.8 m. Over this period, the marginal-ice cluster remains relatively compact in the scatter space. In spring, the AF increases alongside ice thickening, with thicker ice in June, followed by a more dispersed summer state. In September, both AF and SIT decrease again. The seasonal cycle of the MIZ starts again in October, with a sharp reduction of mean SIT while preserving a similar AF. The pack-ice cluster (semi-transparent markers) also displays a C-shaped distribution mirroring that of the MIZ, although with a larger-amplitude structure, with mean SIT spanning from approximately 1.2 m to nearly 3 m, and AF generally exceeding 0.5. The clearest difference between the two regimes occurs throughout the year except during summer, whereas

https://doi.org/10.5194/egusphere-2026-4349
Preprint. Discussion started: 25 August 2026

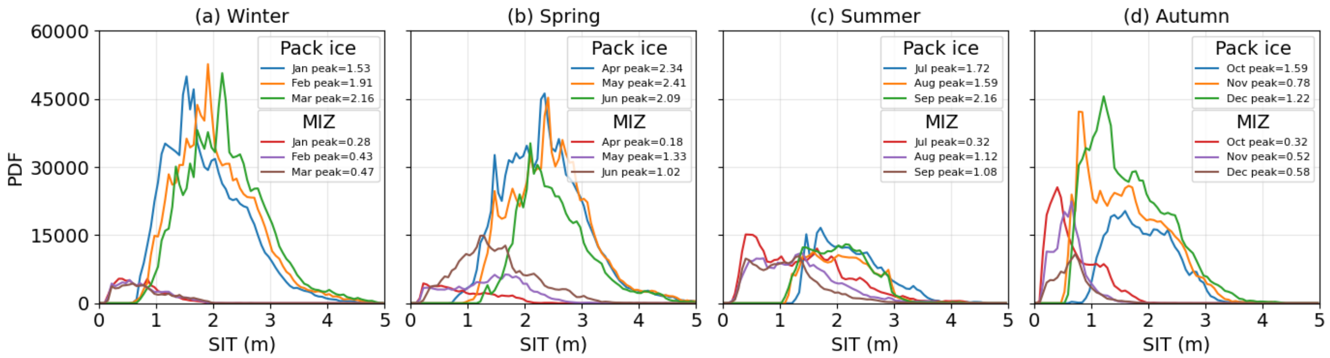

Figure 5. Probability density function (PDF) of pack and marginal ice SIT from GREP climatology in the period 1993–2020. Legends within plots indicate the primary peaks of the distributions.

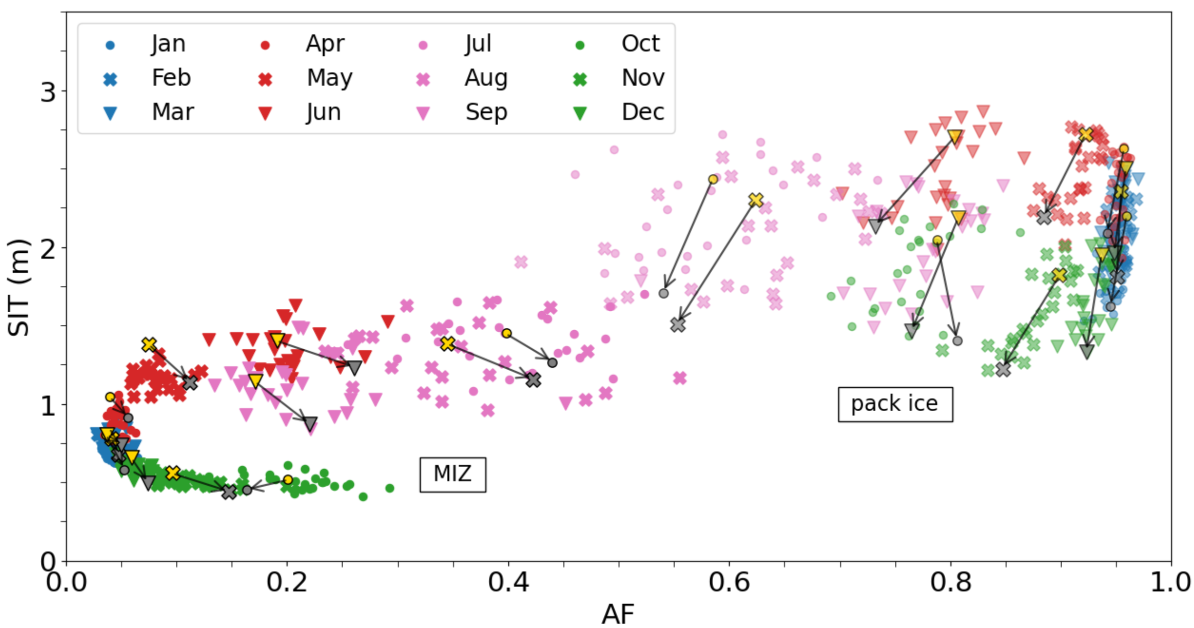

Figure 6. Scatter plot of monthly mean SIT versus AF for the MIZ (solid colors) and pack ice (semi-transparency). Colors and symbols distinguish seasons and months as indicated in the legend. Gold and gray markers represent the first and the last years of the analyzed period (1993–2020), respectively, with black arrows connecting corresponding months.

only partial overlap emerges during July and August, when MIZ and pack ice can occupy similar fractional areas and exhibit comparable thickness values. This overlap reflects the summer transition of part of the pack ice into MIZ conditions, leading the MIZF to include relatively thick first-year ice.

https://doi.org/10.5194/egusphere-2026-4349
Preprint. Discussion started: 25 August 2026

A comparison between the first (1993) and last (2020) years of the record shows a systematic shift of the summer and autumn markers toward the center of the scatter space, i.e. between May and November, indicating that the long-term thinning of pack ice and the concurrent expansion of the MIZ are progressively reducing the separation between the two regimes during the melt season. In October, sea-ice thinning is combined with a decrease in MIZ and an increase in pack-ice AF, reflecting high interannual variability likely associated with Arctic cyclones (Serreze, 2009; Hutter et al., 2019; Blanchard-Wrigglesworth et al., 2022). From December to April, by contrast, the dominant signal remains the thinning of pack ice rather than a major reorganization of AF. Although only two years are shown for clarity, the tendency to populate the central scatter space is representative of a long-term shift associated with the expansion of summer MIZ. The progressive shift of the SIT-AF space suggests that the historical distinction between pack ice and marginal ice is becoming less pronounced during summer, consistent with the transition toward an overall thinner and more seasonal ice.

3.2 Ocean temperature at the sea ice-ocean interface

To complement the analysis of ice thickness and extent, we next examine the thermal conditions of the ocean beneath the ice cover. At the pan-Arctic scale, GREP reveals a clear contrast between SST below pack and marginal ice (Fig. 7). Ocean temperatures under pack ice are consistently colder, generally ranging from about -1.8°C to -1°C, whereas temperatures under the MIZ span a substantially wider interval, from about -1.4°C to 0°C. This contrast is spatially coherent throughout the seasonal cycle. Under the pack ice, the warmer winter temperatures are found in the Laptev and East Siberian Seas, while the coldest conditions occur in the central Arctic (north of the Barents Sea) and in the Chukchi Sea. During summer, SSTs beneath pack ice remain close to the freezing temperature (-1.8°C) only in the region north of the Barents Sea. In contrast, the SST in the MIZ exhibits a pronounced horizontal gradient that increases from the pack-ice edge toward the open ocean. This gradient is strongest during summer, when the MIZ reaches its maximum spatial extent, and weakest in winter, when the MIZ contracts (i.e., a stronger gradient coincides with a wider MIZ).

The time evolution of monthly mean SST beneath the total ice cover (excluding regions with SIC < 0.15), pack ice, and the MIZ is shown in Fig. 8, alongside their corresponding seasonal cycles. SST beneath pack ice exhibits modest seasonal and interannual variability, with minima in April and maxima between July and August, and only a slight long-term warming trend of less than 0.01°C/decade. In contrast, SST beneath the MIZ is characterized by substantially stronger variability. Although the annual SST maximum and minimum timing is similar to that of the pack ice, the MIZ also presents a secondary temperature peak in October, when the MIZ migrates southward to encompass coastal regions of the Beaufort and Siberian seas, cf. Fig. 7. Notably, the SST beneath the MIZ exhibits two distinct trend periods. From 1993 to 2009, the SST shows a weak cooling trend of -0.05 ± 0.02°C/decade, followed by rapid warming from 2010 onward at a rate of 0.33 ± 0.08°C/decade, primarily driven by enhanced summer warming, which reaches 0.70 ± 0.23°C/decade in July. When averaged over the full ice-covered domain (i.e., total ice), SST closely follows conditions of the pack ice in winter, but is strongly influenced by MIZ conditions in summer. As a consequence, the warming trend over the last decade beneath the entire ice cover (0.15 ± 0.07°C/decade) is approximately half of that observed within the MIZ.

https://doi.org/10.5194/egusphere-2026-4349
Preprint. Discussion started: 25 August 2026

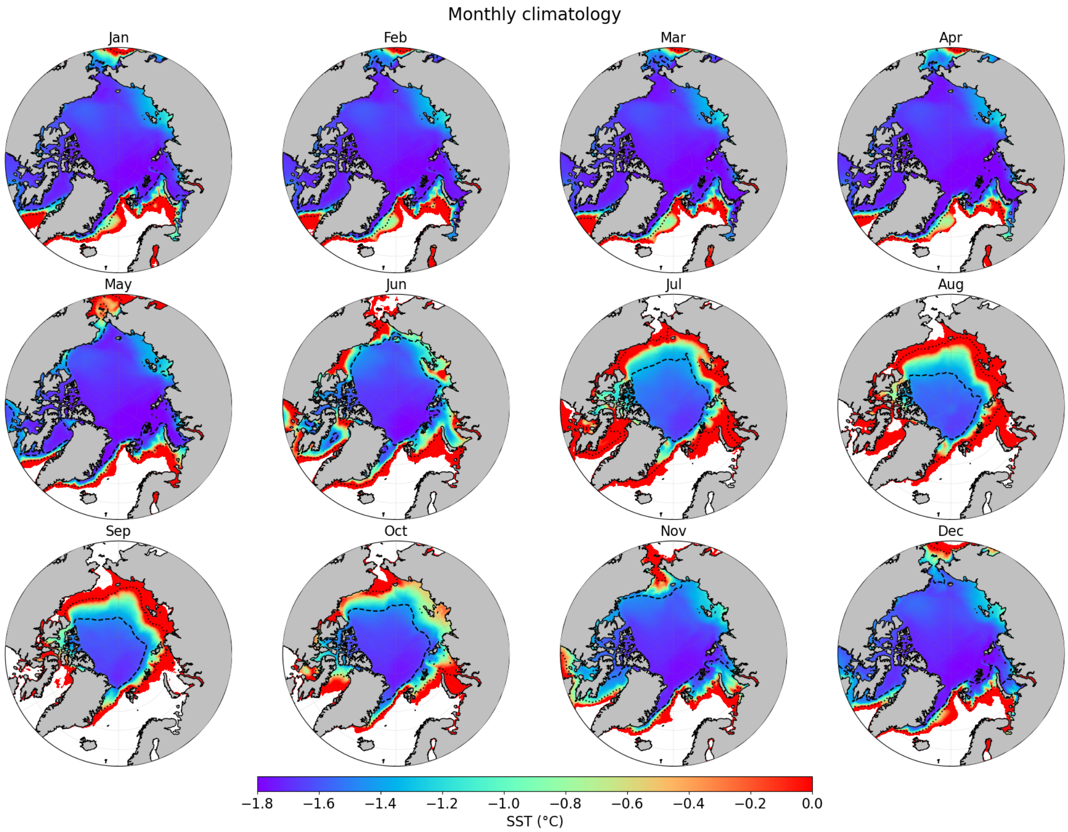

Figure 7. Maps of SST beneath sea ice from GREP climatology in the period 1993-2019. Dashed and dotted lines depict the contours where sea ice concentration climatology is equal to 0.80 and 0.15, respectively.

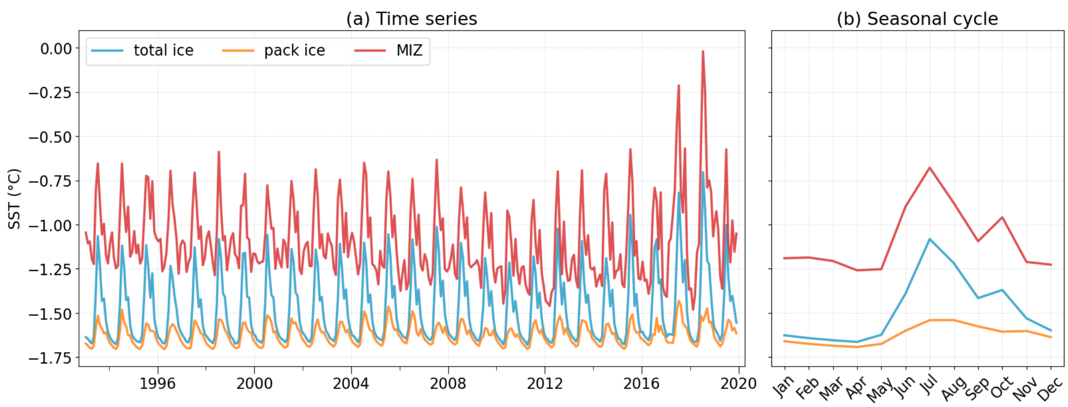

Figure 8. (a) Time series and (b) seasonal cycle of monthly-averaged SST beneath the total ice, pack ice, and the MIZ from GREP in the period 1993-2019.

https://doi.org/10.5194/egusphere-2026-4349
Preprint. Discussion started: 25 August 2026

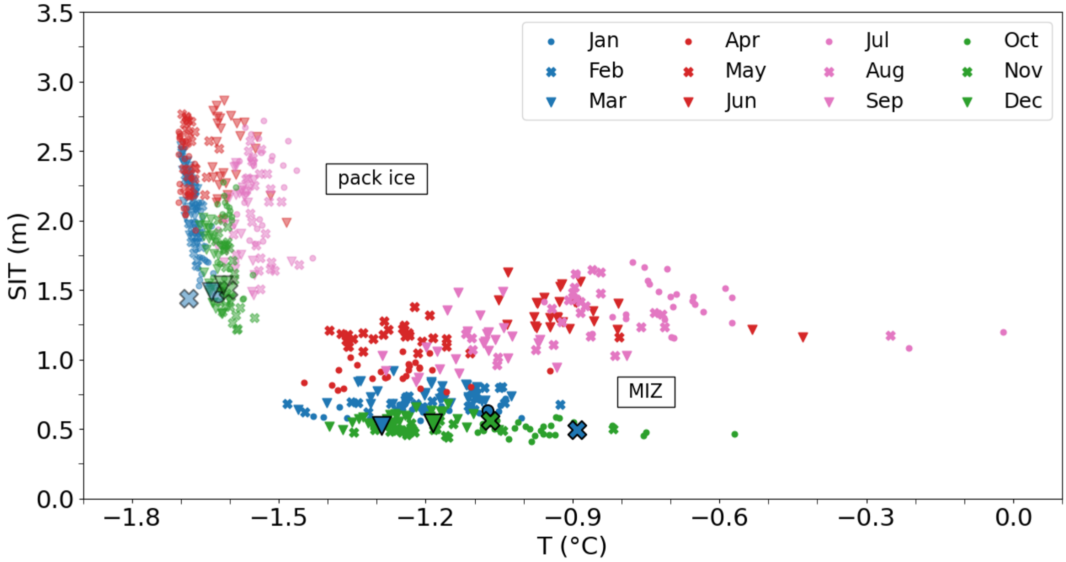

Figure 9. Scatter plot of monthly SST beneath sea ice versus SIT for the MIZ (solid colors) and pack ice (partial transparency) from GREP in the period 1993-2019. Colors and symbols distinguish seasons and months as indicated in the legend. Larger markers are plotted by merging the available sea-ice thickness from CryoSat-2 with the sea surface temperature from OISST in 2017.

The relationship between SIT and SST in Fig. 9 reveals an even clearer separation between pack ice and the MIZ than that identified using the area fraction. Pack ice is generally thicker and characterized by colder, less variable underlying ocean temperature, ranging from approximately -1.70 to -1.40°C. In contrast, the MIZ is associated to thinner ice and warmer, significantly more variable, SST conditions that span a broad interval of nearly 1.5°C. This contrast holds when comparing sea ice–ocean conditions within the same season, with the notable exception of summer, when MIZ sea ice can occasionally exceed pack-ice thickness despite warmer underlying waters. In addition, the thickness distribution is slightly broader for pack ice, extending beyond 1.5 m. The seasonal evolution of the two clusters also differs markedly. In the MIZ, SIT increases gradually from autumn to late spring, accompanied by a decrease in SST that is primarily limited to October and November. A clear shift occurs in June, when both SIT and SST increase relative to the previous month, and this transition leads into the broad and highly dispersed summer cluster. September also exhibits pronounced spatial variability in SIT. By contrast, the seasonal evolution of pack ice is dominated by thickness changes, with progressive thickening from autumn to early spring and thinning during summer, while SST remains relatively constrained throughout the year. Observation-based estimates derived from CryoSat-2 SIT and OISST SST for 2017 support the general structure of the GREP-derived SIT–SST relationship. The observed markers fall close to the GREP scatter space during the growth season, particularly for pack ice, indicating that the reanalysis captures the main characteristics of coupled ocean–sea-ice variability at the pan-Arctic scale.

Overall, the hemispheric-scale analysis shows that SIT variability differs fundamentally between pack ice and the MIZ, that the long-term thinning of Arctic sea ice is accompanied by a progressive convergence of pack and marginal ice characteristics

https://doi.org/10.5194/egusphere-2026-4349
Preprint. Discussion started: 25 August 2026

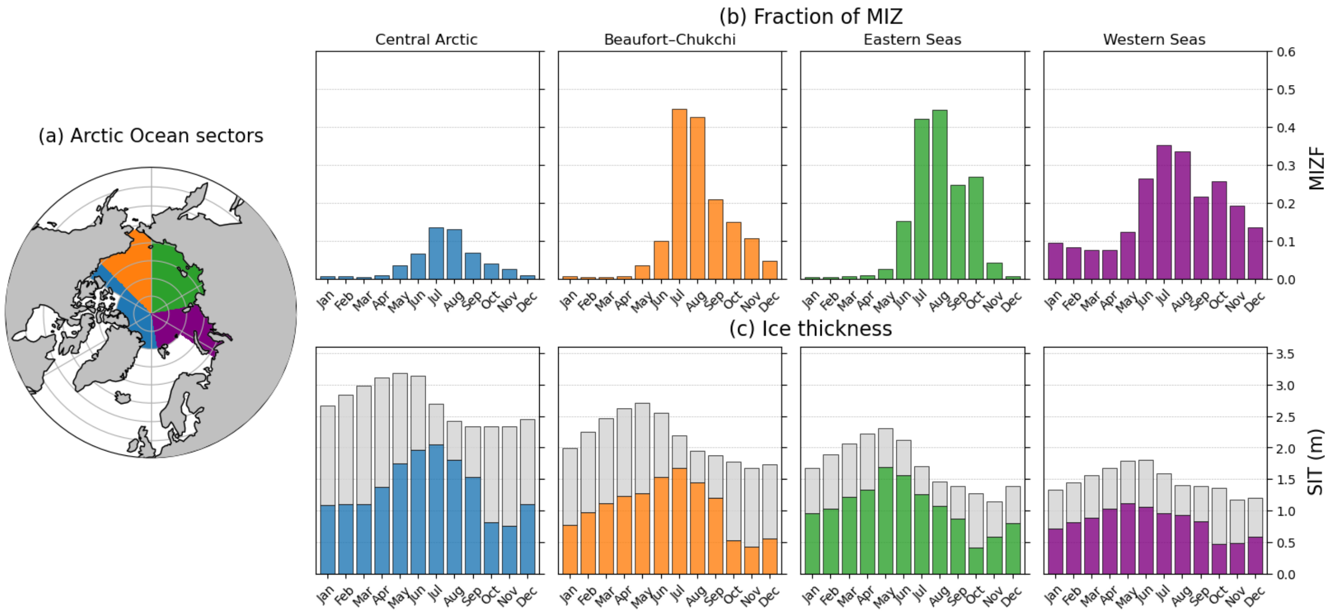

Figure 10. Map of the Arctic sectors used for the regional analysis (a). Seasonal cycles of MIZF (b) and mean SIT (c) for the selected sectors from GREP over the period 1993-2020. In the histograms in panel (c), MIZ thickness is shown in color, while pack-ice SIT is shown in gray.

during summer, and that SST beneath sea ice is systematically warmer and more variable in the MIZ than under pack ice, providing a clearer separation between the two regimes than area-based metrics alone. These results suggest that jointly analyzing sea-ice thickness and upper-ocean conditions offers a useful diagnostic for identifying and characterizing evolving marginal-ice conditions in a warming Arctic.

4 Regional-scale results

Recent changes in the Arctic system exhibit marked spatial heterogeneity (Peng and Meier, 2017; Yang et al., 2023), with specific regions warming significantly faster than others (Yang et al., 2023; Bianco et al., 2024). Next, we examine GREP sea-ice and surface ocean properties within four sectors characterized by distinct MIZ behaviors: Central Arctic, Beaufort-Chukchi, Eastern Seas, and Western Seas (Fig. 10a). This framework is designed to capture regional differences in the development of the MIZ shaped by distinct combinations of ice persistence, seasonal retreat, and oceanic heat influence, and to clarify how regional processes modulate the hemispheric-scale signal.

4.1 Regional regimes of pack ice and the MIZ

The regional contrasts in the seasonal cycle of the MIZ are highlighted in Fig. 10b, which shows the monthly progression of MIZF across the Arctic sectors. The Central Arctic shows the weakest MIZ signal. The sea ice in this region is thick, compact,

https://doi.org/10.5194/egusphere-2026-4349
Preprint. Discussion started: 25 August 2026

and exhibits limited seasonal variability. The MIZ is nearly absent from December to April and remains confined to a short summer season, when MIZF barely exceeds 0.1 in July/August. This sector, therefore, represents the most stable pack-ice regime in the Arctic. The Beaufort–Chukchi sector is also characterized by pack-ice conditions during winter and spring, but undergoes a much stronger seasonal transition than the Central Arctic. In summer, the MIZ expands rapidly, with MIZF exceeding 0.4 in July and August, before contracting in late summer. The MIZ is still present throughout the autumn. This seasonal behavior reflects the strong sensitivity of the region to melt-driven fragmentation and enhanced Pacific inflow through the Bering Strait (Woodgate and Peralta-Ferriz, 2021). The Eastern Seas, encompassing mainly the Laptev and East Siberian seas, share common seasonal characteristics with the Beaufort-Chukchi sector. The most distinctive feature of this sector is the secondary, step-like peak in MIZF in September–October, which indicates pronounced formation of new marginal ice from open water during September and October. The Eastern Seas, therefore, combine a strong summer MIZ signal with a marked autumn re-establishment of marginal conditions. The Western Seas, including a portion of the Barents Sea and the Kara Sea, present the most MIZ-dominated regime. Sea ice in this sector is strongly affected by Atlantic water inflow and is subject to large seasonal variability, leading to partially ice-free summers. Unlike in the other regions, the MIZ is present year-round, with summer maxima above 0.3 and minima between January and May that remain near 0.1. In this sense, the Western Seas represent the Arctic sector most persistently influenced by marginal-ice conditions.

These differences in MIZ seasonality are mirrored by the regional distributions of SIT in Fig. 10c. The Central Arctic contains the thickest pack ice and the largest bias between pack and marginal ice, whereas the Western Seas contain the thinnest ice considering both ice types. The Beaufort-Chukchi and Eastern Seas lie between these two end sectors, combining thick pack ice (greater than 2 m in the yearly maximum) and very thin marginal ice in October. The unique features delineated in Fig. 10b,c indicate that no single region is fully representative of the pan-Arctic signal, although specific regional ice regimes resemble the hemispheric behavior during particular seasons. The Fig. S2 in Supplementary Material complements the analysis, demonstrating that ice thickness PDFs for the regional sectors show marked differences among each other and from the distributions shown in Fig. 5.

4.2 Comparison of regional sea ice thickness with CryoSat-2 observations

The seasonal cycles of mean thickness are compared with CryoSat-2 during the growth season to evaluate the regional representation of SIT in GREP. Their relative bias (expressed as a percentage difference) is displayed in Fig. 11, distinguishing between total ice, pack ice, and the MIZ. Since the MIZ occupies only a small fraction of the regional ice cover in winter (Fig. 10b), the mean MIZ thickness is derived from a limited number of grid cells, making the regional average more sensitive to local variability. To address this limitation, crosses mark whether the uncertainties in CryoSat-2 SIT monthly climatology are larger than the biases between the satellite data and GREP.

At the regional scale, the magnitude and sign of the biases vary substantially. In the Central Arctic, where winter sea ice is overwhelmingly pack ice, GREP shows relatively small differences for both total and pack ice, but tends to underestimate MIZ thickness from November on. In the Beaufort–Chukchi sector, GREP exhibits the largest positive bias in total and pack ice, especially in the middle of the growth season, whereas the MIZ is generally underestimated except in October. In the Eastern

https://doi.org/10.5194/egusphere-2026-4349
Preprint. Discussion started: 25 August 2026

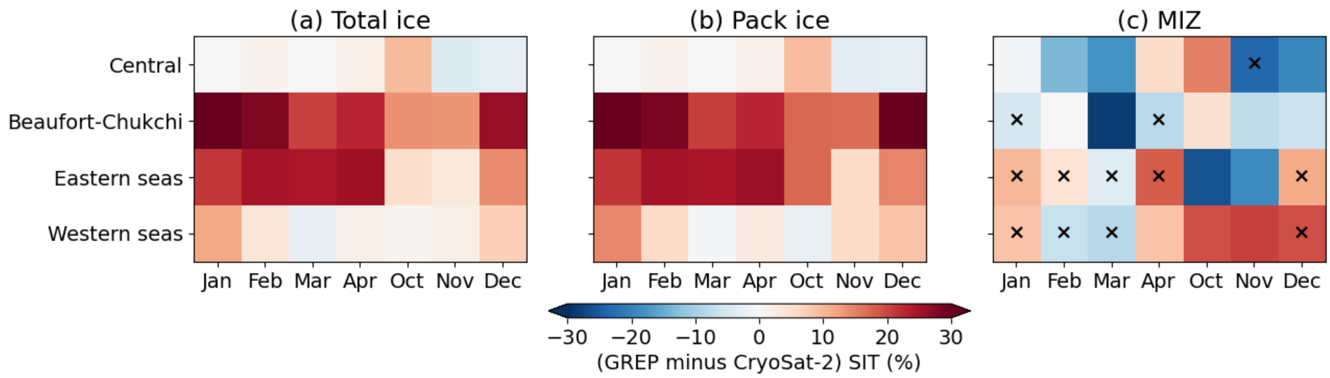

Figure 11. Seasonal cycle of monthly mean SIT differences between GREP and CryoSat-2 (in percentage) during the growth season over the decade 2011–2020, accounting for the availability of satellite-based observations. Panels show results for total (a), pack (b), and the MIZ (c) in the Arctic Ocean sectors. Crosses indicate whether uncertainties in CryoSat-2 SIT monthly climatology are larger than the differences between GREP and CryoSat-2.

Seas, total and pack ice also exhibit positive biases, although weaker than in the Beaufort-Chukchi sector, while the MIZ alternates between positive and negative deviations depending on the month. Finally, the Western Seas only show modest biases in total and pack ice (the maximum in January), whereas the MIZ exhibits a strong and persistent early-season overestimation, the highest among all sectors, followed by a sign reversal in February and March. Overall, GREP captures the broad regional contrast between thick, persistent pack ice and thinner, more variable marginal ice, while retaining region-dependent biases that must be considered when interpreting absolute SIT values.

4.3 Regional SIT-AF structure and long-term trends

The regional scatter plots of mean SIT versus AF further clarify how the contrast between pack ice and the MIZ varies across the Arctic (Fig. 12). Here, AF is consistently computed by accounting for the relative areas of the pack ice and the MIZ within each specific sector. In all sectors, the two regimes remain distinguishable, but the degree of separation differs substantially. The detachment is particularly pronounced in the Central Arctic, where pack ice remains close to AF saturation and occupies a distinct high-thickness cluster, while the MIZ is confined to a much smaller and seasonally limited part of the scatter space. This reflects the persistence of a compact, multiyear pack-ice regime and the relatively minor role of marginal ice in this sector. In the other sectors, the separation between the pack ice and the MIZ remains clear during most of the year, but the overlap increases in summer when the MIZ expands and includes relatively thick first-year ice derived from the fragmentation and melt of the pack ice; occasionally, the MIZ even dominates the pack ice-covered area (i.e., representing the largest AF). The extent of overlap between the clusters characterizes the sectors. In early autumn, the MIZ shifts back toward lower thickness values, reflecting the formation of new marginal ice while MIZ fractions remain relatively large. Regarding the pack ice, the Central Arctic, Beaufort–Chukchi, and Eastern Seas sectors are characterized by near-saturated AF from autumn through

https://doi.org/10.5194/egusphere-2026-4349
Preprint. Discussion started: 25 August 2026

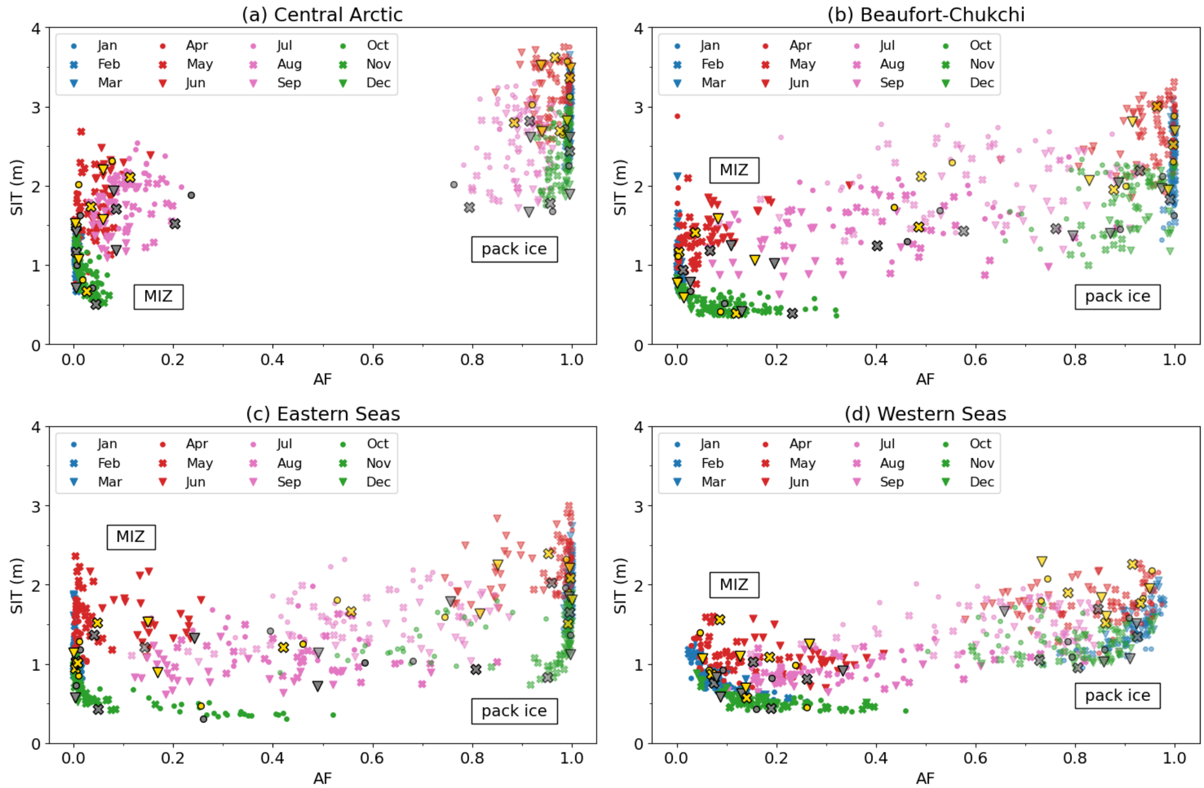

Figure 12. Scatter plots of monthly mean SIT versus AF for MIZ (solid colors) and pack ice (semi-transparency) from GREP displayed for the selected Arctic sectors. Colors and symbols distinguish seasons and months as indicated in the legend. Gold and gray markers represent, respectively, the first and the last years of the analyzed period (1993–2020).

spring. Conversely, the Western Seas sector reaches saturation exclusively during winter and early spring. This reduction in pack ice coverage aligns with the rapid expansion of the MIZ, where the MIZF attains values of up to 0.4 by June.

The comparison between the first (1993) and last (2020) years of the GREP record indicates that the pack ice has become thinner across all Arctic sectors, and, beyond winter and early spring, tends to occupy lower AF values than at the beginning of the period. In parallel, the MIZ generally expands and also shifts toward lower thickness. This transition is most evident in the Central Arctic, Eastern Seas, and Western Seas, where the pack-ice cluster progressively moves toward conditions that more closely resemble the marginal regime. The Beaufort-Chukchi sector shows the same general tendency, though the cluster displacement is less pronounced. While this comparison focuses on the start and end of the period, it is representative of the long-term evolution across the Arctic, as demonstrated in Fig. 13, which presents the long-term changes in AF and SIT.

The decadal trends in sea-ice conditions (measured by the AF) in Fig. 13a vary significantly throughout the year and across different Arctic sectors. The MIZF increases during summer in all regions, with peaks in August–September, while the pack-ice AF decreases correspondingly. The fastest MIZ expansion occurs in the Eastern Seas, at a rate of 0.11 and 0.12 decade^{-1} in

https://doi.org/10.5194/egusphere-2026-4349
Preprint. Discussion started: 25 August 2026

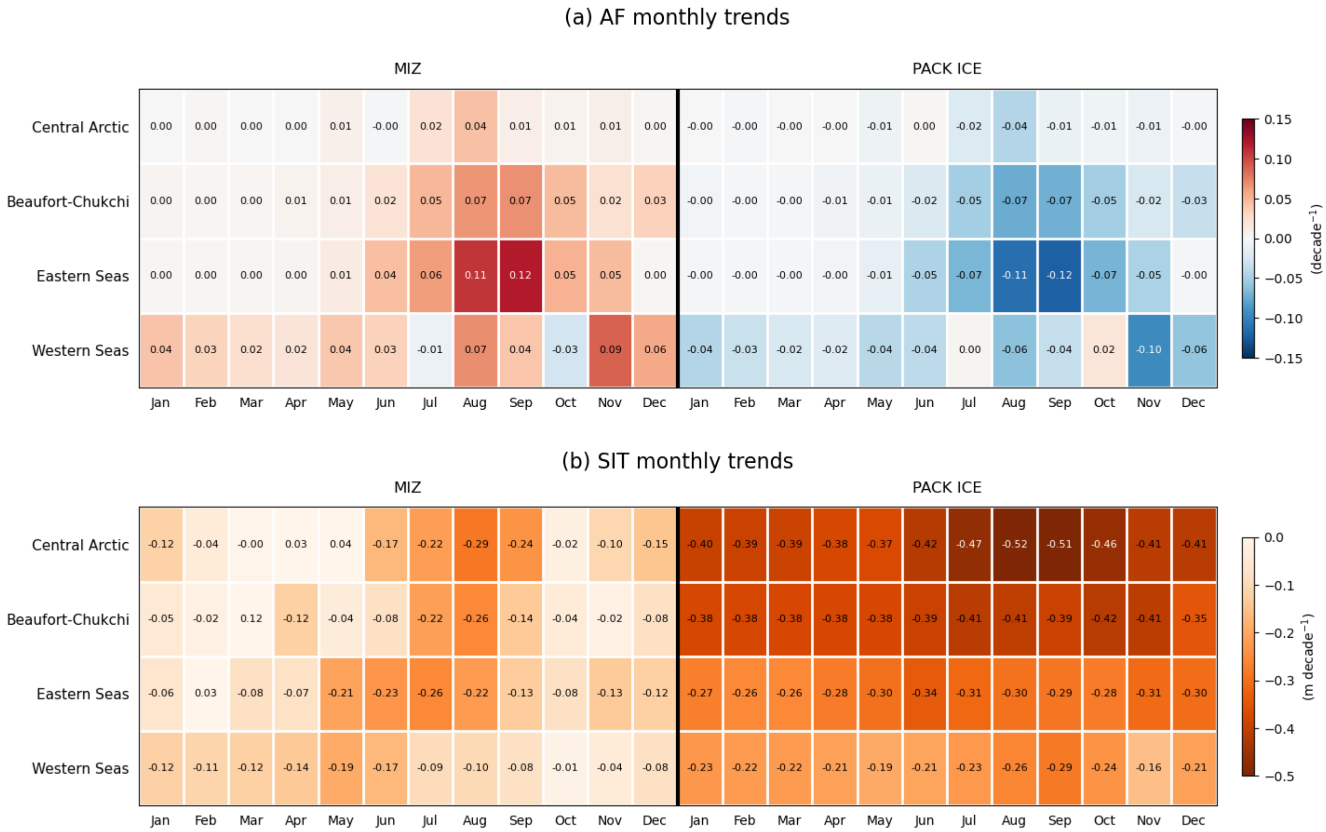

Figure 13. Monthly decadal trends of AF (a) and mean SIT (b) for the MIZ and pack ice from GREP over 1993–2020 for the selected Arctic sectors.

August and September, respectively. Possibly, the role that this sector played in the 2007 and 2017 sea ice minima drives this signal. The Western Seas show positive MIZF trends for most of the year, with the exception of July and October, confirming the persistent strengthening of marginal conditions in that sector. By contrast, the Central Arctic shows the weakest increase in MIZF, with the maximum rate reaching 0.04 decade^{-1}, consistent with its continued dominance by pack ice.

Although sea-ice thinning is observed across all sectors and seasons (Fig. 13b), its magnitude exhibits stronger regional variability than that of AF, with the timing of the annual peak depending on the ice regime and location. The largest decadal trends in MIZ SIT occur in August in the Central Arctic (-0.29 m/decade) and the Beaufort–Chukchi sector (-0.26 m/decade), though the entire season is affected by significant negative trends. In the Eastern Seas, the annual peak is advanced to July (-0.26 m/decade); however, a noticeable MIZ thinning trend persists across all months from May to August. In the Western Seas sector, the peak occurs in May (-0.19 m/decade). This seasonal shift from west to east reflects the different timing of melt, retreat, and ocean influence across the Arctic. In the pack ice, the decadal thinning is stronger than in the MIZ in all sectors, but generally less variable in time. The largest pack-ice thinning is found in the Central Arctic, where rates reach about

https://doi.org/10.5194/egusphere-2026-4349
Preprint. Discussion started: 25 August 2026

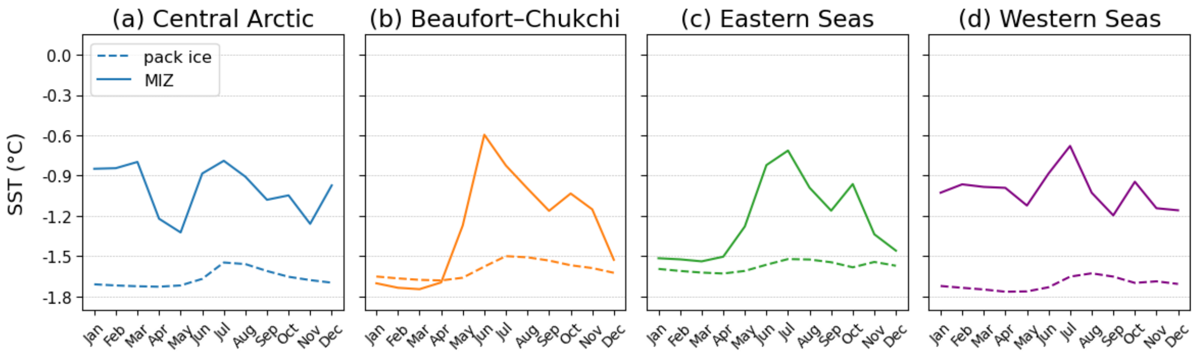

Figure 14. Seasonal cycles of monthly mean SST beneath pack ice (dashed lines) and the MIZ (solid lines) for the selected Arctic sectors, computed from GREP over the period 1993–2019.

−0.50 m/decade between July and October. In the remaining sectors, pack-ice thinning is more homogeneous throughout the year, affecting the Beaufort–Chukchi at rates similar to the Central Arctic, except during the latter's peak months. Lower thinning rates are found in the Western and Eastern Seas sectors.

4.4 Regional variability of ocean surface temperature and SIT-SST relationship

The regional analysis of surface ocean temperature reveals much stronger spatial diversity beneath the MIZ than beneath the pack ice. The seasonality of mean SST beneath marginal and pack ice is shown in Fig. 14 for the four Arctic sectors. Beneath pack ice, the seasonal cycle is broadly similar across regions, with spring minima (April–May), summer maxima (July–August), and a relatively limited annual amplitude. In all regions, rapid warming is observed from the annual minimum to the maximum, whereas the subsequent cooling phase is more gradual. Secondary SST maxima occur in the Eastern and Western Seas sectors in November, likely coinciding with periods of intensified Atlantic Water transport. In contrast, the seasonal cycles of mean SST beneath marginal ice differ substantially across regions in both their evolution and temperature ranges. Only the Beaufort–Chukchi and Eastern Seas sectors show comparable behavior, although the former exhibits a larger seasonal amplitude. Both regions feature late-winter minima in March, a dominant peak between June and July, and a secondary maximum in October. In the Eastern Seas sector, this secondary SST peak occurs one month earlier than beneath the pack ice and coincides with a maximum in the MIZF seasonal cycle (cf. Fig. 10b). Conversely, the Central Arctic sector exhibits two annual minima (April and November) and two maxima (March and July). The Western Seas sector is characterized by a primary summer maximum and a secondary autumn peak (similar to the Beaufort–Chukchi and Eastern Seas sectors), with the lowest temperatures occurring in September.

Regional differences are also evident in the SST trends shown in Fig. 15. In all regions, SST beneath the MIZ exhibits a cooling trend during summer and early autumn (July–October), consistent with the progressive northward shift of the MIZ. During this period, surface cooling ranges from about −0.12 to −0.24°C/decade. From December to June, however, the SST shows positive trends whose intensity strongly depends on the sector considered. The strongest winter warming occurs in

https://doi.org/10.5194/egusphere-2026-4349
Preprint. Discussion started: 25 August 2026

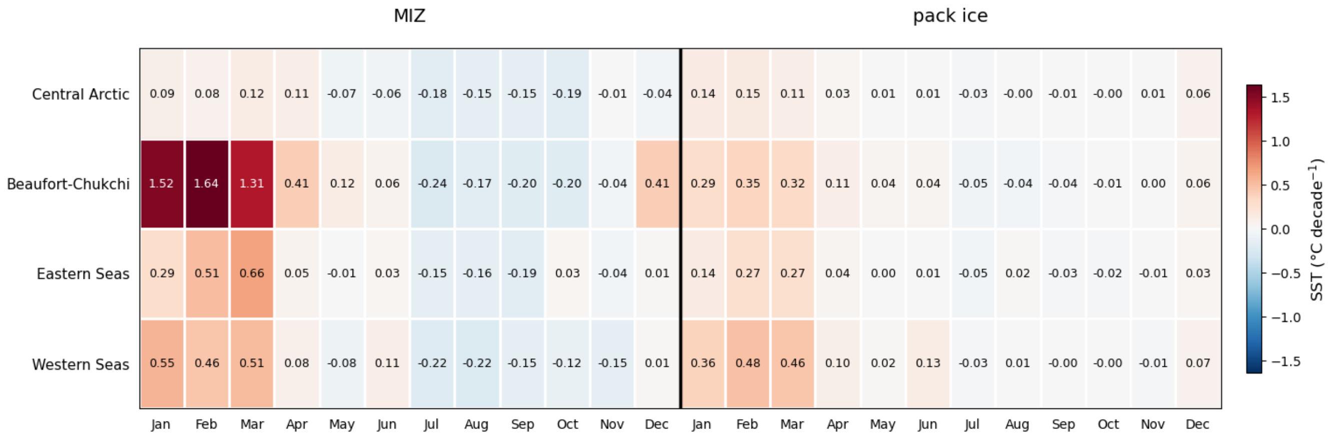

Figure 15. Decadal trends of monthly mean SST beneath the MIZ and pack ice across the selected Arctic sectors, derived from GREP for the 1993–2019 period.

the Beaufort–Chukchi sector, where SST trends exceed 1.3°C/decade between January and March, and reach approximately 0.4°C/decade in December and April. In the Eastern and Western Seas, winter warming below the MIZ is also pronounced (0.29 to 0.66°C/decade), whereas the Central Arctic shows weaker warming, consistent with the smaller MIZ extent. Beneath pack ice, SST trends are more regionally homogeneous and much weaker (absolute values below 0.05°C/decade) through most of the melt season, with only moderate warming in June within the Western Seas. Between December and April, SST exhibits a warming trend across all sectors, peaking primarily in February and March. The strongest increase occurs in the Western Seas, where the warming rate reaches nearly 0.5°C/decade at its maximum.

The relationship between SIT and SST retains the broad pan-Arctic contrast between colder pack ice and warmer MIZ conditions, but its regional expression differs substantially among sectors (Fig. 16). In all sectors, the pack ice occupies a relatively narrow SST range and generally corresponds to colder ocean conditions than those of the MIZ. However, the degree of separation between the two regimes varies: the clearest distinction remains in the Central Arctic, where the pack ice is both thick and cold, and in the Western Seas, where the MIZ occupies a wide and relatively warm SST range distinct from the pack-ice cluster. By contrast, greater overlap between the pack and marginal ice is found in the Eastern Seas, particularly in late autumn and winter, whereas in the Beaufort-Chukchi sector, the MIZ spans a broader temperature range with the freezing point as its lower boundary.

The MIZ clusters display significant regional diversity and depart markedly from the pan-Arctic behavior. In autumn, marginal ice in the Beaufort–Chukchi and Western Seas is associated with relatively thin ice and a wide range of SST. In the Eastern Seas, a clearer relationship emerges between cooling SST and increasing MIZ thickness. In the Central Arctic, autumn marginal ice thickens while SST becomes warmer. In winter, sea ice in the MIZ continues to thicken in all sectors except the Central Arctic, where mean SIT values remain close to December conditions. In this region, most marginal ice transitions into pack ice, and the remaining MIZ is associated with comparatively warm SST. Conversely, in the Beaufort–Chukchi and

https://doi.org/10.5194/egusphere-2026-4349
Preprint. Discussion started: 25 August 2026

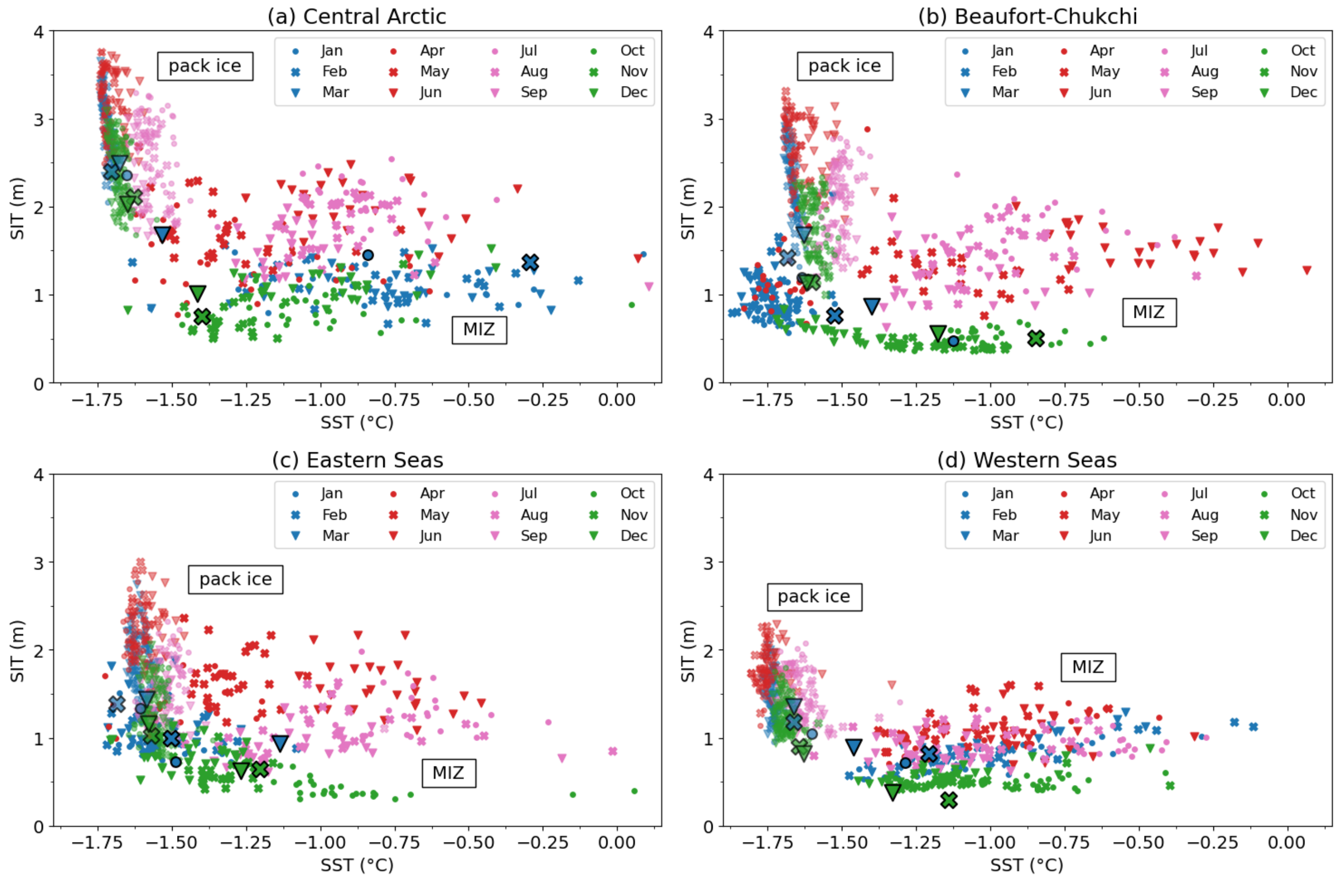

Figure 16. Scatter plots of monthly SST beneath sea ice versus SIT for marginal ice (solid colors) and pack ice (semi-transparent markers) from GREP over the period 1993–2019, shown for the selected Arctic sectors. Colors and symbols distinguish seasons and months as indicated in the legend. Larger markers are plotted by merging the available sea-ice thickness from CryoSat-2 with the sea surface temperature from OISST in 2017.

Eastern Seas sectors, SST beneath the MIZ decreases further, approaching the freezing point, whereas it remains relatively stable or slightly warmer in the Western Seas. During spring and summer, the MIZ spans a broad portion of the SIT-SST space in the Central Arctic, Beaufort–Chukchi, and Eastern Seas sectors, indicating substantial interannual variability. In the first two sectors, the spring and summer clusters partially overlap. In contrast, the Eastern Seas exhibit distinct clusters, where MIZ sea ice in spring is thicker than in summer and occupies a similar temperature range, albeit shifted toward colder values. Finally, the Western Seas show a stronger overlap between winter, spring, and summer MIZ conditions, suggesting weaker seasonal variability in ocean thermal forcing despite changes in ice thickness. Observation-based estimates from OISST and CryoSat-2 for 2017 broadly support the regional GREP-derived SIT–SST relationships. Considering the pack ice, the positions of the observation markers in the scatter space are consistent with GREP across all regions. By contrast, the alignment between the

https://doi.org/10.5194/egusphere-2026-4349
Preprint. Discussion started: 25 August 2026

products is more heterogeneous in the MIZ and depends on the sector and month. Although a fair agreement emerges between GREP and observations, differences among the datasets tend to occur in March, in line with the regional SIT biases already identified in Fig. 11.

Overall, this analysis shows that the SST beneath pack ice is comparatively uniform across the Arctic, whereas the SST beneath the MIZ is strongly region-dependent in its seasonal cycle, long-term trend, and relationship with ice thickness. This confirms that the upper ocean-sea ice coupling is not governed by a single Arctic-wide regime, but reflects the interplay between local ocean heat supply, seasonal ice retreat, and the persistence of marginal conditions. The Central Arctic remains largely pack-ice dominated, the Western Seas represent a persistently marginal and Atlantic-influenced regime, while the Beaufort-Chukchi and Eastern Seas are characterized by strongly seasonal conditions and pronounced summer expansion of the MIZ. These regional contrasts explain why pan-Arctic diagnostics alone are insufficient to capture the processes governing the Arctic variability.

5 Discussion

The results highlight that characterizing Arctic sea ice requires careful selection of both diagnostic metrics and observational datasets, especially given the growing importance of the marginal ice zone (MIZ) in the changing Arctic. As discussed in the Data and Methods section, and illustrated in Fig. 1, the widely used SIE metric is poorly suited to represent the spatial coverage of the MIZ because it does not account for variations in sea ice concentration. By contrast, SIA provides a more realistic measure of the actual ice-covered area. For pack ice, where ice concentrations remain close to 100%, SIE and SIA are in close agreement, making SIE a reasonable proxy for spatial coverage. The representation of the MIZ is also challenged by the lower agreement among available SIT observational products than over consolidated pack ice, further highlighting the difficulties in measuring ice thickness during the melt season. By contrast, the spatial and temporal consistency of GREP enables the characterization of MIZ thickness variability and its relationship with upper-ocean properties, despite its members not directly assimilating SIT observations. While the pan-Arctic representation of the MIZ in GREP has previously been evaluated using concentration-based metrics (Cocetta et al., 2024), the present analysis extends the focus to SIT, providing new insight into the relationships among different sea ice metrics.

Although the seasonal and multiannual variabilities of SIT differ markedly between pack ice and the MIZ, their monthly probability density functions (PDFs) derived from GREP over 1993–2020 exhibit similar shapes during summer (cf. Fig. 5), albeit over different SIT ranges. Summer similarities between pack ice and the MIZ also emerge when relating ice thickness to the fraction of sea-ice cover. Figure 6 shows that, while the scatter distributions are well separated for most of the year, they converge under summer conditions as a result of recent pack-ice thinning and MIZ expansion. This convergence suggests that Arctic sea-ice variability is increasingly controlled by transitional ice regimes. Rather than representing a peripheral component of the ice cover, the MIZ is becoming a major contributor to the seasonal evolution of Arctic sea ice. This transition implies that future Arctic change may be governed less by variations in consolidated pack ice and increasingly by processes operating within seasonal and MIZ regimes. In contrast, when relating SIT to ocean surface temperature, the scatter distributions of pack

https://doi.org/10.5194/egusphere-2026-4349
Preprint. Discussion started: 25 August 2026

ice and the MIZ remain well separated, as shown in Fig. 9. This reflects the distinct properties of the underlying ocean, with SST beneath pack ice being noticeably colder than beneath the MIZ. Such a separation indicates that upper-ocean thermal conditions provide information that is complementary to area-based metrics. While the present analysis does not establish causality, the coherent evolution of SIT and SST supports the interpretation that ocean heat availability is closely linked to the MIZ conditions.

The regional analysis accounts for the spatial variability of sea ice by dividing the Arctic Ocean into four sectors. This framework captures the seasonal variability of the MIZF in terms of both distribution shape and peak intensity. Analysis of mean SIT across these sectors (Fig. 10) revealed that the timing of maximum SIT in the MIZ shifts from May to July, progressing from the MIZ-dominated Western Seas to the largely MIZ-free Central Arctic, while all sectors exhibit minimum SIT in October–November. In contrast, SIT in the pack ice displays a broadly consistent seasonal shape, revealing the stable nature of pack ice compared to the MIZ, which is more sensitive to coupled ocean dynamics and atmospheric forcing.

The scatter plots relating SIT to AF across Arctic sectors (Fig. 12) indicate that no single region is fully representative of pan-Arctic sea-ice conditions. However, specific regional distributions exhibit similarities to hemispheric-scale behavior. For instance, the MIZ behavior in the Western Seas resembles the pan-Arctic MIZ pattern, while pack ice in the Central Arctic and Beaufort–Chukchi sectors is more representative of overall Arctic conditions. These results suggest that regional processes all contribute differently to the hemispheric-scale signal and that no single dominant process governs MIZ variability. Monthly decadal trends in SIT (Fig. 13) further highlight this variability, with the largest negative trends shifting from May to August when moving from the Western Seas to the Central Arctic, a shift that is broadly consistent with the pathways of Atlantic Water circulation as it enters the Arctic Ocean. This suggests that ocean heat transport contributes substantially to the evolution of Arctic marginal ice conditions, although its relative role varies across sectors.

Finally, as shown in Fig. 14, we found that SST beneath the MIZ exhibits pronounced regional variability, unlike the strong similarities observed across Arctic sectors beneath the pack ice. In sectors where the MIZF exhibits a pronounced summer peak (Beaufort–Chukchi and Eastern Seas), the surface ocean warms earlier and shows a secondary SST maximum in October. This feature contributes to the re-establishment of marginal ice in the Eastern Seas, while in the Beaufort–Chukchi sector, it delays the transition back to pack-ice conditions. In the Western Seas, where the MIZ persists year-round, SST beneath marginal ice displays enhanced seasonal variability driven by local processes and ocean heat transport. These regional features are further reflected when relating SIT with SST across the Arctic sectors in Fig. 16. The scatter plots emphasize the complex coupling between sea-ice thickness and surface ocean temperatures.

6 Conclusions

We presented a pan-Arctic and regional assessment of the spatiotemporal variability of the Arctic MIZ that integrates sea-ice thickness and its link with upper ocean properties. By combining satellite observations and ocean reanalyses, this study provides a pan-Arctic and regional characterization of Arctic MIZ thickness variability, recognizing the large discrepancies among available SIT estimates. A close examination of the metrics used to quantify sea-ice cover revealed the large uncertainties associated with the widely used SIE when evaluating the MIZ, highlighting the need for diagnostic metrics specifically suited to characterize the evolving Arctic sea-ice cover.

The widening of the Arctic marginal ice zone and the concurrent reduction in sea-ice thickness represent key indicators of the ongoing transition toward a seasonally dominated Arctic ice cover. These changes have direct implications for the Arctic climate state, as they characterize the changing coupling between the ocean and sea ice. The strong regional contrasts identified in this study indicate that future Arctic change cannot be adequately described using pan-Arctic metrics alone. Instead, regional MIZ processes and their interaction with the upper ocean are likely to become increasingly important drivers of Arctic climate variability. These findings suggest that the MIZ and its thickness should be considered key indicators of Arctic climate change alongside more traditional metrics such as sea-ice extent. Improving the representation and monitoring of MIZ processes in observational systems, reanalyses, and Earth System Models will therefore be essential for constraining future projections of the Arctic climate state.

Code and data availability

The four-member GREP ensemble is no longer available online; however, these datasets are available from the corresponding author upon reasonable request. Data from GREP members have been individually downloaded from the institutions' websites. The remaining observational datasets used in this study are publicly available. The CryoSat-2 product was retrieved from the Alfred Wegener Institute (AWI) FTP server (ftp.awi.de:/sea_ice/product/cryosat2/v2p6/nh/l3c_grid/), as was the SMOS dataset (ftp://ftp.awi.de:21/sea_ice/product/smos/v3.6/nh/). The merged CryoSat-2/Sentinel-3/SMOS product was obtained from the repository (ftp://ftp.awi.de/sea_ice/product/cryosat2_smos/v300/nh/). Year-round sea-ice thickness estimates based on CryoSat-2 were accessed via the British Antarctic Survey repository (https://ramadda.data.bas.ac.uk/repository/entry/show?entryid=synth:d8c66670-57ad-44fc-8fef-942a46734ecb:L0RldmVsb3BlcnNfUHJvZHVjdA==, last access: May 2026). Finally, the NOAA high-resolution OISST ocean temperature data were downloaded from the NCAR Climate Data Guide (https://climatedataguide.ucar.edu/climate-data/sst-data-noaa-high-resolution-025x025-blended-analysis-daily-sst-and-ice-oisstv2, last access: May 2026).

Decadal trends and associated statistical significance were computed using the linregress function from the scipy.stats module of the SciPy Python library (Virtanen et al., 2020). The analysis scripts are available from the corresponding author upon request.

Author contributions

FC and DI wrote the manuscript. FC analyzed simulated and observed datasets. DI conceived the study. All authors contributed to the interpretation of results and edited and reviewed the manuscript.

https://doi.org/10.5194/egusphere-2026-4349
Preprint. Discussion started: 25 August 2026

Competing interests

The contact author has declared that none of the authors has any competing interests.

Financial Support

This research was supported by the European Union via the ObsSea4Clim (Ocean observations and indicators for climate and assessments) project (grant Agreement number 101136548) and the Marine Environment Reanalyses Evaluation Project – MER-EP.

https://doi.org/10.5194/egusphere-2026-4349
Preprint. Discussion started: 25 August 2026

References

Babb, D. G., Galley, R. J., Kirillov, S., Landy, J. C., Howell, S. E. L., Stroeve, J. C., Meier, W., Ehn, J. K., and Barber, D. G.: The Stepwise Reduction of Multiyear Sea Ice Area in the Arctic Ocean Since 1980, Journal of Geophysical Research: Oceans, 128, https://doi.org/10.1029/2023jc020157, 2023.

Banzon, V., Reynolds, R., and for Atmospheric Research Staff, N. C.: The Climate Data Guide: SST data: NOAA High-resolution (0.25° × 0.25°) Blended Analysis of Daily SST and Ice (OISSTv2), https://climatedataguide.ucar.edu/climate-data/sst-data-noaa-high-resolution-025x025-blended-analysis-daily-sst-and-ice-oisstv2, last modified 9 September 2022, 2022.

Bianco, E., Iovino, D., Masina, S., Materia, S., and Ruggieri, P.: The role of upper-ocean heat content in the regional variability of Arctic sea ice at sub-seasonal timescales, The Cryosphere, 18, 2357–2379, https://doi.org/10.5194/tc-18-2357-2024, 2024.

Blanchard-Wrigglesworth, E., Webster, M., Boisvert, L., Parker, C., and Horvat, C.: Record Arctic Cyclone of January 2022: Characteristics, Impacts, and Predictability, Journal of Geophysical Research: Atmospheres, 127, https://doi.org/10.1029/2022jd037161, 2022.

Cipollone, A., Banerjee, D. S., Iovino, D., Aydogdu, A., and Masina, S.: Bivariate sea-ice assimilation for global-ocean analysis–reanalysis, Ocean Science, 19, 1375–1392, https://doi.org/10.5194/os-19-1375-2023, 2023.

Cocetta, F., Zampieri, L., Selivanova, J., and Iovino, D.: Assessing the representation of Arctic sea ice and the marginal ice zone in ocean–sea ice reanalyses, The Cryosphere, 18, 4687–4702, https://doi.org/10.5194/tc-18-4687-2024, 2024.

Dawson, G., Landy, J., Tsamados, M., Komarov, A. S., Howell, S., Heorton, H., and Krumpen, T.: A 10-year record of Arctic summer sea ice freeboard from CryoSat-2, Remote Sensing of Environment, 268, 112 744, https://doi.org/10.1016/j.rse.2021.112744, 2022.

Desportes, C., Drévillon, M., Clavier, M., and Gounou, A.: PRODUCT USER MANUAL For the Global Ocean Reanalysis Product GLOBAL-REANALYSIS-PHY-001-026 Issue: 1.6, https://catalogue.marine.copernicus.eu/documents/PUM/CMEMS-GLO-PUM-001-026.pdf, 2022.

Donlon, C., Robinson, I., Casey, K. S., Vazquez-Cuervo, J., Armstrong, E., Arino, O., Gentemann, C., May, D., LeBorgne, P., Piollé, J., Barton, I., Beggs, H., Poulter, D. J. S., Merchant, C. J., Bingham, A., Heinz, S., Harris, A., Wick, G., Emery, B., Minnett, P., Evans, R., Llewellyn-Jones, D., Mutlow, C., Reynolds, R. W., Kawamura, H., and Rayner, N.: The Global Ocean Data Assimilation Experiment High-resolution Sea Surface Temperature Pilot Project, Bulletin of the American Meteorological Society, 88, 1197–1214, https://doi.org/10.1175/bams-88-8-1197, 2007.

Edel, L., Xie, J., Korosov, A., Brajard, J., and Bertino, L.: Reconstruction of Arctic sea ice thickness (1992–2010) based on a hybrid machine learning and data assimilation approach, The Cryosphere, 19, 731–752, https://doi.org/10.5194/tc-19-731-2025, 2025.

Emery, W. J., Baldwin, D. J., Schlüssel, P., and Reynolds, R. W.: Accuracy of in situ sea surface temperatures used to calibrate infrared satellite measurements, Journal of Geophysical Research: Oceans, 106, 2387–2405, https://doi.org/10.1029/2000jc000246, 2001.

European Union-Copernicus Marine Service: Global Ocean Ensemble Physics Reanalysis, https://doi.org/10.48670/MOI-00024, 2019.

Ezraty, R., Girard-Ardhuin, F., Piollé, J. F., Kaleschke, L., and Heygster, G.: Arctic and Antarctic Sea Ice Concentration and Arctic Sea Ice Drift Estimated from Special Sensor Microwave Data, Département d'Océanographie Physique et Spatiale, IFREMER, Brest, France and University of Bremen Germany 2, 2007.

Fichefet, T. and Maqueda, M. A. M.: Sensitivity of a global sea ice model to the treatment of ice thermodynamics and dynamics, Journal of Geophysical Research: Oceans, 102, 12 609–12 646, https://doi.org/10.1029/97jc00480, 1997.

Frew, R. C., Bateson, A. W., Feltham, D. L., and Schröder, D.: Toward a marginal Arctic sea ice cover: changes to freezing, melting and dynamics, The Cryosphere, 19, 2115–2132, https://doi.org/10.5194/tc-19-2115-2025, 2025.

https://doi.org/10.5194/egusphere-2026-4349
Preprint. Discussion started: 25 August 2026

Goosse, H. and Fichefet, T.: Importance of ice-ocean interactions for the global ocean circulation: A model study, Journal of Geophysical Research: Oceans, 104, 23 337–23 355, https://doi.org/10.1029/1999jc900215, 1999.

Goosse, H., Kay, J. E., Armour, K. C., Bodas-Salcedo, A., Chepfer, H., Docquier, D., Jonko, A., Kushner, P. J., Lecomte, O., Massonnet, F., Park, H.-S., Pithan, F., Svensson, G., and Vancoppenolle, M.: Quantifying climate feedbacks in polar regions, Nature Communications, 9, https://doi.org/10.1038/s41467-018-04173-0, 2018.

Hendricks, S. and Paul, S.: Product User Guide & Algorithm Specification - AWI CryoSat-2 Sea Ice Thickness (version 2.6) Issued by, https://doi.org/10.5281/ZENODO.10044554, 2023.

Horvat, C.: Marginal ice zone fraction benchmarks sea ice and climate model skill, Nature Communications, 12, 2221, https://doi.org/10.1038/s41467-021-22004-7, 2021.

Horvat, C., Blanchard-Wrigglesworth, E., and Petty, A.: Observing Waves in Sea Ice With ICESat-2, Geophysical Research Letters, 47, https://doi.org/10.1029/2020gl087629, 2020.

Huang, B., Liu, C., Banzon, V., Freeman, E., Graham, G., Hankins, B., Smith, T., and Zhang, H.-M.: Improvements of the Daily Optimum Interpolation Sea Surface Temperature (DOISST) Version 2.1, Journal of Climate, 34, 2923–2939, https://doi.org/10.1175/jcli-d-20-0166.1, 2021.

Hunke, E. C. and Dukowicz, J. K.: An Elastic–Viscous–Plastic Model for Sea Ice Dynamics, Journal of Physical Oceanography, 27, 1849–1867, https://doi.org/10.1175/1520-0485(1997)027<1849:aevpmf>2.0.co;2, 1997.

Hunke, E. C. and Lipscomb, W. H.: CICE: The sea ice model documentation and software user's manual, version 4.1, Technical report, LA-CC-06-012, Los Alamos National Laboratory: Los Alamos, NM, 2010.

Huntemann, M., Heygster, G., Kaleschke, L., Krumpen, T., Mäkynen, M., and Drusch, M.: Empirical sea ice thickness retrieval during the freeze-up period from SMOS high incident angle observations, The Cryosphere, 8, 439–451, https://doi.org/10.5194/tc-8-439-2014, 2014.

Hutter, N., Zampieri, L., and Losch, M.: Leads and ridges in Arctic sea ice from RGPS data and a new tracking algorithm, The Cryosphere, 13, 627–645, https://doi.org/10.5194/tc-13-627-2019, 2019.

Iovino, D., Selivanova, J., Masina, S., and Cipollone, A.: The Antarctic Marginal Ice Zone and Pack Ice Area in CMEMS GREP Ensemble Reanalysis Product, Frontiers in Earth Science, 10, https://doi.org/10.3389/feart.2022.745274, 2022.

Kaleschke, L., Maaß, N., Haas, C., Hendricks, S., Heygster, G., and Tonboe, R. T.: A sea-ice thickness retrieval model for 1.4 GHz radiometry and application to airborne measurements over low salinity sea-ice, The Cryosphere, 4, 583–592, https://doi.org/10.5194/tc-4-583-2010, 2010.

Kaleschke, L., Tian-Kunze, X., Maas, N., Ricker, R., Hendricks, S., and Drusch, M.: Improved retrieval of sea ice thickness from SMOS and CryoSat-2, in: 2015 IEEE International Geoscience and Remote Sensing Symposium (IGARSS), p. 5232–5235, IEEE, https://doi.org/10.1109/igarss.2015.7327014, 2015.

Landy, J. C., Dawson, G. J., Tsamados, M., Bushuk, M., Stroeve, J. C., Howell, S. E. L., Krumpen, T., Babb, D. G., Komarov, A. S., Heorton, H. D. B. S., Belter, H. J., and Aksenov, Y.: A year-round satellite sea-ice thickness record from CryoSat-2, Nature, 609, 517–522, https://doi.org/10.1038/s41586-022-05058-5, 2022.

Lavergne, T., Sørensen, A. M., Kern, S., Tonboe, R., Notz, D., Aaboe, S., Bell, L., Dybkjær, G., Eastwood, S., Gabarro, C., Heygster, G., Killie, M. A., Brandt Kreiner, M., Lavelle, J., Saldo, R., Sandven, S., and Pedersen, L. T.: Version 2 of the EUMETSAT OSI SAF and ESA CCI sea-ice concentration climate data records, The Cryosphere, 13, 49–78, https://doi.org/10.5194/tc-13-49-2019, 2019.

https://doi.org/10.5194/egusphere-2026-4349
Preprint. Discussion started: 25 August 2026

Lellouche, J.-M., Galloudec, O. L., Drévillon, M., Régnier, C., Greiner, E., Garric, G., Ferry, N., Desportes, C., Testut, C.-E., Bricaud, C., Bourdallé-Badie, R., Tranchant, B., Benkiran, M., Drillet, Y., Daudin, A., and De Nicola, C.: Evaluation of global monitoring and forecasting systems at Mercator Océan, Ocean Science, 9, 57–81, https://doi.org/10.5194/os-9-57-2013, 2013.

Liu, A., Yang, J., Bao, Q., Vitart, F., Liu, J., Liang, X., Lu, M., Kim, S.-J., Gong, D., Tian, Z., and Liu, H.: Assimilating summer sea ice thickness enhances predictions of Arctic sea ice and surrounding atmosphere within two months, npj Climate and Atmospheric Science, 8, https://doi.org/10.1038/s41612-025-01050-8, 2025.

MacLachlan, C., Arribas, A., Peterson, K. A., Maidens, A., Fereday, D., Scaife, A. A., Gordon, M., Vellinga, M., Williams, A., Comer, R. E., Camp, J., Xavier, P., and Madec, G.: Global Seasonal forecast system version 5 (GloSea5): a high-resolution seasonal forecast system, Quarterly Journal of the Royal Meteorological Society, 141, 1072–1084, https://doi.org/10.1002/qj.2396, 2014.

Mangatane, M. J., Iovino, D., Santi, f. D., Cocetta, F., and Vichi, M.: Contribution of Young Ice Formation Processes to the Simulation of Antarctic Sea ice Mass Budget, https://doi.org/10.22541/essoar.176306477.77217476/v1, 2025.

Matthews, J. L., Peng, G., Meier, W. N., and Brown, O.: Sensitivity of Arctic Sea Ice Extent to Sea Ice Concentration Threshold Choice and Its Implication to Ice Coverage Decadal Trends and Statistical Projections, Remote Sensing, 12, 807, https://doi.org/10.3390/rs12050807, 2020.

Mignac, D., Martin, M., Fiedler, E., Blockley, E., and Fournier, N.: Improving the Met Office's Forecast Ocean Assimilation Model (FOAM) with the assimilation of satellite-derived sea-ice thickness data from CryoSat-2 and SMOS in the Arctic, n/a, https://doi.org/10.1002/qj.4252, 2022.

Notz, D.: Sea-ice extent and its trend provide limited metrics of model performance, The Cryosphere, 8, 229–243, https://doi.org/10.5194/tc-8-229-2014, 2014.

OSI SAF: Global Sea Ice Concentration Climate Data Record v3.0 - Multimission, https://doi.org/10.15770/EUM_SAF_OSI_0013, 2022.

Peng, G. and Meier, W. N.: Temporal and regional variability of Arctic sea-ice coverage from satellite data, Annals of Glaciology, 59, 191–200, https://doi.org/10.1017/aog.2017.32, 2017.

Perovich, D. K., Richter-Menge, J. A., Jones, K. F., and Light, B.: Sunlight, water, and ice: Extreme Arctic sea ice melt during the summer of 2007, Geophysical Research Letters, 35, https://doi.org/10.1029/2008gl034007, 2008.

Ricker, R., Hendricks, S., Helm, V., Skourup, H., and Davidson, M.: Sensitivity of CryoSat-2 Arctic sea-ice freeboard and thickness on radar-waveform interpretation, The Cryosphere, 8, 1607–1622, https://doi.org/10.5194/tc-8-1607-2014, 2014.

Ricker, R., Hendricks, S., Kaleschke, L., Tian-Kunze, X., King, J., and Haas, C.: A weekly Arctic sea-ice thickness data record from merged CryoSat-2 and SMOS satellite data, The Cryosphere, 11, 1607–1623, https://doi.org/10.5194/tc-11-1607-2017, 2017.

Rolph, R. J., Feltham, D. L., and Schröder, D.: Changes of the Arctic marginal ice zone during the satellite era, The Cryosphere, 14, 1971–1984, https://doi.org/10.5194/tc-14-1971-2020, 2020.

Selivanova, J., Iovino, D., and Cocetta, F.: Past and future of the Arctic sea ice in High-Resolution Model Intercomparison Project (HighResMIP) climate models, The Cryosphere, 18, 2739–2763, https://doi.org/10.5194/tc-18-2739-2024, 2024.

Serreze, M.: Northern Hemisphere Cyclone Locations and Characteristics from NCEP/NCAR Reanalysis Data, Version 1, https://doi.org/10.5067/XEPCLZKPAJBK, 2009.

Simon, A., Tandeo, P., Sévellec, F., and Lique, C.: Arctic regional changes revealed by clustering of sea-ice observations, The Cryosphere, 19, 6639–6658, https://doi.org/10.5194/tc-19-6639-2025, 2025.

https://doi.org/10.5194/egusphere-2026-4349
Preprint. Discussion started: 25 August 2026

Storto, A., Masina, S., and Navarra, A.: Evaluation of the CMCC eddy-permitting global ocean physical reanalysis system (C-GLORS, 1982–2012) and its assimilation components, Quarterly Journal of the Royal Meteorological Society, 142, 738–758, https://doi.org/10.1002/qj.2673, 2016.

Sumata, H., de Steur, L., Divine, D. V., Granskog, M. A., and Gerland, S.: Regime shift in Arctic Ocean sea ice thickness, Nature, 615, 443–449, https://doi.org/10.1038/s41586-022-05686-x, 2023.

Tian-Kunze, X., Kaleschke, L., Maaß, N., Mäkynen, M., Serra, N., Drusch, M., and Krumpen, T.: SMOS-derived thin sea ice thickness: algorithm baseline, product specifications and initial verification, The Cryosphere, 8, 997–1018, https://doi.org/10.5194/tc-8-997-2014, 2014.

Tilling, R. L., Ridout, A., and Shepherd, A.: Near-real-time Arctic sea ice thickness and volume from CryoSat-2, The Cryosphere, 10, 2003–2012, https://doi.org/10.5194/tc-10-2003-2016, 2016.

Vancoppenolle, M., Bopp, L., Madec, G., Dunne, J., Ilyina, T., Halloran, P. R., and Steiner, N.: Future Arctic Ocean primary productivity from CMIP5 simulations: Uncertain outcome, but consistent mechanisms, Global Biogeochemical Cycles, 27, 605–619, https://doi.org/10.1002/gbc.20055, 2013.

Vichi, M.: An indicator of sea ice variability for the Antarctic marginal ice zone, The Cryosphere, 16, 4087 – 4106, https://doi.org/doi.org/10.5194/tc-16-4087-2022, 2022.

Virtanen, P., Gommers, R., Oliphant, T. E., Haberland, M., Reddy, T., Cournapeau, D., Burovski, E., Peterson, P., Weckesser, W., Bright, J., van der Walt, S. J., Brett, M., Wilson, J., Millman, K. J., Mayorov, N., Nelson, A. R. J., Jones, E., Kern, R., Larson, E., Carey, C. J., Polat, I., Feng, Y., Moore, E. W., VanderPlas, J., Laxalde, D., Perktold, J., Cimrman, R., Henriksen, I., Quintero, E. A., Harris, C. R., Archibald, A. M., Ribeiro, A. H., Pedregosa, F., van Mulbregt, P., Vijaykumar, A., Bardelli, A. P., Rothberg, A., Hilboll, A., Kloeckner, A., Scopatz, A., Lee, A., Rokem, A., Woods, C. N., Fulton, C., Masson, C., Häggström, C., Fitzgerald, C., Nicholson, D. A., Hagen, D. R., Pasechnik, D. V., Olivetti, E., Martin, E., Wieser, E., Silva, F., Lenders, F., Wilhelm, F., Young, G., Price, G. A., Ingold, G.-L., Allen, G. E., Lee, G. R., Audren, H., Probst, I., Dietrich, J. P., Silterra, J., Webber, J. T., Slavič, J., Nothman, J., Buchner, J., Kulick, J., Schönberger, J. L., de Miranda Cardoso, J. V., Reimer, J., Harrington, J., Rodríguez, J. L. C., Nunez-Iglesias, J., Kuczynski, J., Tritz, K., Thoma, M., Newville, M., Kümmerer, M., Bolingbroke, M., Tartre, M., Pak, M., Smith, N. J., Nowaczyk, N., Shebanov, N., Pavlyk, O., Brodtkorb, P. A., Lee, P., McGibbon, R. T., Feldbauer, R., Lewis, S., Tygier, S., Sievert, S., Vigna, S., Peterson, S., More, S., Pudlik, T., Oshima, T., Pingel, T. J., Robitaille, T. P., Spura, T., Jones, T. R., Cera, T., Leslie, T., Zito, T., Krauss, T., Upadhyay, U., Halchenko, Y. O., and Vázquez-Baeza, Y.: SciPy 1.0: fundamental algorithms for scientific computing in Python, Nature Methods, 17, 261–272, https://doi.org/10.1038/s41592-019-0686-2, 2020.

Warren, S. G., Rigor, I. G., Untersteiner, N., Radionov, V. F., Bryazgin, N. N., Aleksandrov, Y. I., and Colony, R.: Snow Depth on Arctic Sea Ice, Journal of Climate, 12, 1814–1829, https://doi.org/10.1175/1520-0442(1999)012<1814:sdoasi>2.0.co;2, 1999.

Woodgate, R. A. and Peralta-Ferriz, C.: Warming and Freshening of the Pacific Inflow to the Arctic From 1990-2019 Implying Dramatic Shoaling in Pacific Winter Water Ventilation of the Arctic Water Column, Geophysical Research Letters, 48, https://doi.org/10.1029/2021gl092528, 2021.

Yang, M., Qiu, Y., Huang, L., Cheng, M., Chen, J., Cheng, B., and Jiang, Z.: Changes in Sea Surface Temperature and Sea Ice Concentration in the Arctic Ocean over the Past Two Decades, Remote Sensing, 15, 1095, https://doi.org/10.3390/rs15041095, 2023.

Zuo, H., Balmaseda, M. A., Tietsche, S., Mogensen, K., and Mayer, M.: The ECMWF operational ensemble reanalysis–analysis system for ocean and sea ice: a description of the system and assessment, Ocean Science, 15, 779–808, https://doi.org/10.5194/os-15-779-2019, 2019.

https://doi.org/10.5194/egusphere-2026-4349
Preprint. Discussion started: 25 August 2026

Zygmuntowska, M., Rampal, P., Ivanova, N., and Smedsrud, L. H.: Uncertainties in Arctic sea ice thickness and volume: new estimates and implications for trends, The Cryosphere, 8, 705–720, https://doi.org/10.5194/tc-8-705-2014, 2014.